

**Please cite the Published Version**

Beake, BD, Harris, AJ, Liskiewicz, TW, Wagner, J, McMaster, SJ, Goodes, SR, Neville, A and Zhang, L (2021) Friction and electrical contact resistance in reciprocating nano-scale wear testing of metallic materials. *Wear*, 474-5. p. 203866. ISSN 0043-1648

**DOI:** <https://doi.org/10.1016/j.wear.2021.203866>

**Publisher:** Elsevier

**Version:** Accepted Version

**Downloaded from:** <https://e-space.mmu.ac.uk/627483/>

**Usage rights:**  [Creative Commons: Attribution-Noncommercial-No Derivative Works 4.0](https://creativecommons.org/licenses/by-nc-nd/4.0/)

**Additional Information:** Published by and copyright Elsevier.

**Enquiries:**

If you have questions about this document, contact [openresearch@mmu.ac.uk](mailto:openresearch@mmu.ac.uk). Please include the URL of the record in e-space. If you believe that your, or a third party's rights have been compromised through this document please see our Take Down policy (available from <https://www.mmu.ac.uk/library/using-the-library/policies-and-guidelines>)

**Friction and electrical contact resistance in reciprocating nano-scale wear testing of  
metallic materials**

Ben D. Beake<sup>1,\*</sup>, Adrian J. Harris<sup>1</sup>, Tomasz W. Liskiewicz<sup>2</sup>, Jérémie Wagner<sup>3</sup>, Sam J.  
McMaster<sup>4</sup>, Stephen R. Goodes<sup>1</sup>, Anne Neville<sup>4</sup> and Lei Zhang<sup>5</sup>

1 Micro Materials Ltd., Willow House, Ellice Way, Yale Business Village, Wrexham, LL13  
7YL, UK

2 John Dalton Building, Faculty of Science and Engineering, Manchester Metropolitan  
University, Chester Street, Manchester M15 6BH, UK

3 Ecole Nationale d'Ingénieurs de Metz, 1 route d'Ars Laquenexy BP 65820, 57078 Metz,  
cedex 3, France

4 School of Mechanical Engineering, University of Leeds, Woodhouse Lane, Leeds LS2 9JT,  
UK

5 State Key Laboratory for Powder Metallurgy, Central South University, Changsha 410083,  
China

\*Corresponding author: e-mail: [ben@micromaterials.co.uk](mailto:ben@micromaterials.co.uk)

Keywords: micro-wear, biomaterials, electrical contact resistance, reciprocating nano-wear

**Abstract**

Reciprocating contacts occur in a wide variety of practical wear situations including hip joints and electrical contacts. In developing tribological tests for candidate materials with improved durability in these contacts it is beneficial that the contact conditions (e.g. sliding speed) can be reproduced. Hence, a fully instrumented capability for rapid high-cycle linear reciprocating nano-scale wear tests has been developed. It is multi-sensing with high data

acquisition measurements of probe displacement data, friction, cumulative frictional energy dissipation and electrical contact resistance. **In comparison with other nanoindenters** the design has the high level of lateral rigidity which provides sufficient stability to perform nano- or micro-scale wear tests for extended duration (e.g. several hours, up to 300 m sliding). In this study, reciprocating nano-wear tests with diamond probes have been performed on the biomedical alloys Ti6Al4V and 316L stainless steel, and with electrically conductive metallic probes on gold and silver alloys. The stainless steel exhibited a ductile response with low friction throughout the load range. At higher loads on Ti6Al4V, there was an abrupt transition to higher friction and fracture-dominated wear after ~20 cycles. Improved detection of the onset of wear and the subsequent failure mechanisms sliding against conductive probes was possible by a multi-sensing approach simultaneously monitoring friction and electrical contact resistance (ECR). Changes in ECR exhibited a complex correlation with changes to the measured friction. The reciprocating tests of noble metal-noble metal contacts (Au-Au and Ag-Ag) showed much longer endurance than gold vs. steel contacts although occasional isolated failures were observed. A new approach for the analysis of repetitive nano-scratch test data was also developed enabling improved data mining.

## **1. Introduction**

Wear begins at the asperities between contacting surfaces but the contact pressures acting on these are not generally known accurately in a standard macro-scale tribological test. In contrast, testing at the nano-/micro-scale (“single asperity tribology”) enables the onset of wear to be studied conveniently and correlations with friction forces can be investigated to aid the design of surfaces with improved wear resistance. The simplified contact conditions in

the single asperity tests enables deconvolution of the individual factors that combine to result in the overall measured friction and wear. With the advent of methods for precision topographic control, e.g. to produce textured surfaces for friction control, there has been an increasing interest in studying the influence of surface topography on friction and wear [1-8]. This can be conveniently studied by nanomechanical tribology (using atomic force microscopes or nanoindenters) but this is typically limited to relatively small number of cycles (<100) and small track lengths of the order of 100  $\mu\text{m}$ . Although the term single-asperity tribology was originally coined for AFM-based methods, the precision polished diamond probes with end radii of a few microns that are used in nano- and micro-scratch tests in nanomechanical instruments can effectively be considered as single asperity contacts. The metrology requirements for performing nano- and micro-scale scratch tests have been reviewed, with high lateral rigidity of the loading head being identified as important to minimise artefacts on rough surfaces [9].

An important development in microtribology is to integrate a capability for high cycle, high speed, high sliding distance reciprocating sliding at the mN level to commercial nanomechanical test instrumentation, where the high lateral rigidity of the loading head is retained together with sensitive friction and depth measurement. This capability could provide a linkage across the length scales usually probed in nano- or macro- scale tribological tests and enable the study of running-in processes in greater detail than possible previously.

In this report we describe this development where, additionally, its multi-sensing capability has been expanded by the incorporation of electrical contact resistance (ECR) measurement during the wear tests. Although the benefits of ECR measurement have been criticized [10] it has generally proved extremely useful, as in fretting tests [11-15]. Echeverrigaray and co-workers reported that ECR monitoring provided a valuable tool for detecting premature wear

of an electrically non-conductive DLC coating sliding against steel in a pin-on-disk test by dielectric breakdown [16].

Case studies have been performed with popular biomedical alloys and on materials used in sliding electrical connectors to benchmark the instrumentation and evaluate its sensitivity and stability for extended testing. Samples chosen for the case studies were (i) Ti6Al4V and 316L stainless steel (ii) multilayer electroplated sliding contacts (iii) bulk silver and gold alloys being developed as sliding contact materials. Ti6Al4V in particular is an important material with use in aerospace and biomedical applications but its tribological performance can be poor so greater understanding of the onset of wear on this alloy may be beneficial in mitigating this. Tribological behaviour of electrical connectors is key to the reliability of electronic systems. Understanding sliding failure due to frequent mating-unmating is important in developing improved connector systems. To achieve low contact resistance the real area of contact must be very high, so soft metals are pushed together at high force and conditions for electrical power contacts are more severe than most tribological contacts resulting in very short lifetimes (low sliding distance to failure) [17]. Tian and co-workers reported a multi-stage deformation in sphere-on-flat reciprocating sliding tests between electroplated gold contacts (Au-Ni vs. Au-Ni) on brass [10]. Typically, the failure was rapid with the top most gold layer removed within 100 cycles and the substrate exposed within ~200 cycles. Although the friction coefficient was sensitive to the wearing away of the different layers the electrical contact resistance was almost constant throughout the sliding test.

Bulk noble metals have shown improved performance compared to the electroplated systems. In this work extended reciprocating tests (~2-46 hr duration) have been performed on bulk gold and silver alloys. The reciprocating tests on a bulk silver alloy were also complemented by 20-cycle repetitive unidirectional scratch tests with a diamond indenter to (i) help

understanding of how wear proceeds in the more complex, higher cycle reciprocating test (ii) help determine whether nano-scratch tests can be designed more efficiently on rough surfaces.

## **2. Instrument development**

Control software was written to enable a reciprocating stage to be controlled independently of the instrument loading head. Two different stages (from NanoMotion and PI) were successfully integrated and controlled within the NanoTest Vantage (Micro Materials Ltd., Wrexham, UK) software. The experimental setup with the PI stage is shown in fig. 1(a). The velocity-time profile is user adjustable but in the following tests it was set so the velocity was constant over 90% of the wear track and linearly reduced to zero at the turn-around points as illustrated in the velocity-time profile shown in fig. 1(b), for a 0.5 mm/s velocity and 5 s trace-retrace cycle duration. Friction was measured throughout the tests allowing the construction of friction loops. The (dynamic) friction coefficient was determined in software from the energy dissipation during full sliding using an approach similar to that employed by Fouvry and Liskiewicz for friction measurement in fretting tests [11-14].

$$\mu = \text{Energy dissipation} / (2 \times \text{track length} \times \text{applied load}) \quad \text{Eqn. [1]}$$

The static friction coefficient is obtained from the static friction using a similar approach to Burris and Sawyer which accounts for any transducer misalignment [18]. The probe displacement is also monitored continuously and recorded over the entire wear track enabling in-situ wear measurements. Several authors have reiterated the potential usefulness in measuring wear in situ rather than relying on post-test profilometry measurements [19,20]. In wear prediction it is often assumed that the wear rate is linear but this is generally not the

case, particularly when there is a change in the predominant wear mechanism during the test [20,21].

Table 1 compares the typical conditions in the new capability for nano-scale reciprocating wear to other approaches for multi-pass sliding contacts (repetitive scratch and nano-fretting) with the same instrumentation. The loading head, load range (0-500 mN, for low load head) and capability for tangential (frictional) force and ECR measurement are common to all three. In the nano-scratch test the combination of high load and smaller probe radii result in high contact pressure (typically  $> 1$  GPa) during the test. In the study of coated systems a key benefit is that the test parameters can be controlled - e.g. in a repetitive sub-critical load test - so that the peak stresses can be placed in the vicinity of the interface, enhancing sensitivity to subtle differences in interfacial bonding strength [22]. In the nano-fretting test the much larger number of cycles that can be conveniently run enables tests at lower stresses (larger radii and/or smaller contact loads). The small track length means that total sliding distance is relatively low but the transition from fretting/partial slip to gross slip can be studied [23,24]. The larger sliding speeds and larger sliding distances in the NanoTriboTest enable longer duration high contact pressure tests. The higher sliding speeds enable more direct replication of those in MEMS contacts [25]. The ECR was measured with a computer controlled National Instruments Dual-Output Power Source-Measure Unit. Electrically conductive probes such as metallic materials or Boron-doped diamond are required for ECR measurement.

The case studies provided sufficient data to (i) evaluate instrumentation stability and suitability for long duration testing (ii) determine suitable data analysis approaches to handle the very large datasets (iii) investigate the correlations between different signals in the multi-sensing tests.

### **3. Experimental**

#### *3.1 Reciprocating wear of 316L stainless steel and Ti6Al4V*

A NanoTest Vantage (Micro Materials Ltd., Wrexham, UK) fitted with a NanoTriboTest module was used for the reciprocating tests. Reciprocating nano-wear experiments were performed on biomedical grade 316L stainless steel and Ti6Al4V alloy samples (supplied by the University of Birmingham, UK) with a diamond indenter of 25  $\mu\text{m}$  end radius. The track length was 1 mm and the maximum sliding velocity was 0.5 mm/s. The velocity was at its maximum over the central 90% of the track and linearly reduced to zero at the turn-around points. The applied loads were 10, 30, 50, 100, 200 and 500 mN on the 316L stainless steel and 20, 30, 40, 50, 70, 100, 200, 500 mN on the Ti6Al4V. For Ti6Al4V some additional tests were performed at 40 mN and above to assess test repeatability/sensitivity to local differences in wear resistance (e.g. due to microstructural variations). The friction force and the raw (unlevelled, uncorrected for any instrumental drift or frame compliance contribution) probe displacements were monitored continuously and recorded over the entire wear track. Final wear depths were also determined by confocal microscopy of wear tracks (Keyence VHX-6000).

#### *3.2 Reciprocating wear of electroplated gold and bulk gold and silver alloys*

In the tests with metallic probes the ECR was also measured. Reciprocating sliding tests were performed at 10 mN between a steel ball of 1 mm radius and the flat surface of a multi-layered sliding electrical connector (layer architecture  $\sim 50$  nm Au/ $\sim 2.5$   $\mu\text{m}$  Ag/nickel underplate/Cu alloy substrate) at a sliding velocity = 2 mm/s and track length = 5 mm. The nickel underplate layer is used as a diffusion barrier between the surface layers (gold and

silver) and the copper substrate. Tests were feedback controlled with a fixed current of 0.1 A and a maximum Voltage of 6 V. To assess the repeatability of the test, six tests were performed under the same conditions.

As scoping tests to assess the stability of the instrumentation to perform extended testing, longer duration and higher load tests were performed with non-axisymmetric noble metal alloy probes sliding against noble metal alloy disks (disks and probes were supplied by Central South University, China). A gold alloy (Au-9wt.%Ni) connector was used as the probe against an Au-20wt.%Ag-Cu10wt.% disk. Two different Ag-20wt.%Cu-2wt.%Ni connectors were used as sliding probes against an Ag-10wt.%Cu disk. The probe used for the shorter test at 50 mN test had a larger equivalent radius of the order of 2 mm. The test conditions in the reciprocating tests with the metallic probes are summarised in Table 2.

### *3.3 Repetitive nano-scratch tests on silver alloy*

Repetitive nano-scratch experiments were performed on an Ag alloy disk (Ag-10wt.%Cu) with a diamond indenter of 18  $\mu\text{m}$  end radius sliding at 5  $\mu\text{m/s}$  over a 1 mm track. Peak loads were 50 and 200 mN with three repeat tests at each load separated by 100  $\mu\text{m}$ . Tests at 200 mN were performed as 41 cycle tests with alternate topography (minimal load, 0.1 mN) and scratch cycles. Tests at 50 mN were 22 cycles, with pre-scratch topography and a post-scratch topography after 20 scratches. The tests were designed with a loading rate to combine sufficient regions of ramped and constant loading in the scratch track. In the initial period of the scratch cycles the load was minimal (0.1 mN) before ramping to reach the peak load (after 100  $\mu\text{m}$  ramped at 0.5 mN/s to 50 mN; after 250  $\mu\text{m}$  ramped at 4 mN/s to 200 mN [see fig. 7(b)]). The initial track region was used for subsequent levelling of the data in the NanoTest software.  $R_a$  surface roughness measured under load and for residual scratch scans. After correcting the displacement data for sample slope and frame compliance in the

NanoTest software, the scratch recovery ( $SR$ ) was determined from the on-load depth ( $h_t$ ) and residual depth ( $h_r$ ) data according to Eqn. 2:-

$$SR = 100\% \times (h_t - h_r) / h_r \quad [\text{Eqn. 2}]$$

Additionally, 3 ramped load scratch tests were performed to 500 mN, loading at 4 mN/s and scanning at 5  $\mu\text{m}$  /s.

## 4. Results

### 4.1 *Ti6Al4V and 316L stainless steel*

The friction force showed some variability over a single cycle which was more evident at lower load, and after a higher number of wear cycles. The mean friction coefficient vs. cycles are shown in figure 2 (a) (for clarity only 4 loads and the first 150 cycles are shown). Typically, over the first few cycles there was a decrease in friction that gradually slowed to reach a final friction coefficient of  $\sim 0.05-0.07$  after 500 cycles. The initial decrease in friction was more pronounced at 500 mN. As the load increases the friction becomes higher around the turnaround points where the velocity is lower, implying that the static friction ( $\mu_{st}$ ) becomes greater than the dynamic friction. This behaviour was first observed towards the end of the 30 mN test ( $\mu_{st} \sim 0.1$ ). Larger static friction values were found in the tests at higher load, which increased with number of cycles ( $\mu_{st} \sim 0.15$  to  $\sim 0.2$  at 50 mN;  $\mu_{st} \sim 0.17$  to  $\sim 0.2$  at 100 mN;  $\mu_{st} \sim 0.17$  to  $\sim 0.38$  at 200 mN;  $\mu_{st} \sim 0.2$  to  $\sim 0.45$  at 500 mN). As an indication of the wear rate, figure 2 (b) shows changes in the displacement value at the mid-point of the track with continued cycling. Corresponding SEM images of the wear tracks reveal ductile behaviour with increasing pile-up at the sides of the wear track at higher load (fig. 2(c,d)).

At low load (20-40 mN) on Ti6Al4V the friction was low throughout the test ( $\mu \sim 0.04-0.05$  at end). At  $\geq 50$  mN the friction was initially low ( $\mu \sim 0.05$ ) but increased after  $\sim 10-20$  cycles to reach high values ( $\mu \sim 0.5$ ) with the transition complete within 2-3 cycles. An example at 100 mN is shown in figure 3(a,b). Energy dissipation per cycle and cumulative energy dissipation are shown in figure 3(c,d). SEM images of wear tracks above and below the transition are shown in figure 4. Friction coefficient results at 30-50 mN on both materials are shown in figure 5 (a). The figure shows there was a marked correlation between friction coefficient and the observed deformation, with low friction for ductile ploughing and a transition to very high friction at 50 mN on Ti6Al4V. Although it was not possible to accurately determine the very low wear depths  $< 50$  mN from confocal imaging the wear depth data at  $\geq 50$  mN shown in figure 5(b) confirmed the greater damage on Ti6Al4V than 316L stainless steel.

#### *4.2 Electroplated gold connector*

Tribological failure of the multi-layered interconnector system proceeded by a multi-stage wear process. Friction and ECR during 70 mm sliding distance segments (i.e. showing 7 cycles) for a typical test are shown in figure 6 (a-d). In this test the first isolated increase (“spike”) in resistance was after  $\sim 340$  mm of sliding. Thereafter occasional isolated spikes in resistance were observed with continued sliding, with electrical failure gradually occurring over more of the 1 mm wear track, but without any noticeable change in friction. Later in the test more of the track fails with marked increase in friction. **The mean friction coefficient and mean resistance per sliding cycle are shown for another test in figure 6(e).** In the initial stage the friction coefficient was around 0.25 and the resistance gradually increased to  $\sim 1 \Omega$  which marks a transition and the friction and resistance increase rapidly (stage 2), reaching a high friction coefficient of  $\sim 0.7$ , thereafter friction and resistance are high and variable (stage 3) with periodic increases and decreases in resistance until (stage 4) further increases in

resistance and slight decrease in friction. The corresponding non-averaged values of the contact resistance for the test shown in fig. 6(e) are shown in figure 6(f). In this test there are some isolated spikes of  $\sim 4 \Omega$  in the first 40 cycles and the spike density increases after 40 cycles.

Although there was some test to test variability in the number of cycles to failure, these features were observed in all bar one test, with a mean resistance of  $\sim 1 \Omega$  marking the transition (fig.6(g)). The initial stage with a gradual increase in ECR was also observed in the other test. It is assumed that the wear process was proceeding more gradually and the other stages would have been observed had the test been continued. Post-test optical microscopy revealed probe wear/debris and fracture-dominated wear tracks.

#### 4.3 Ag alloy scratch tests

In ramped scratches to 500 mN the mean friction coefficient increased with load to reach a maximum value of  $\mu = (0.27 \pm 0.01)$  at 500 mN. The friction coefficient vs. scan cycles determined at 50 mN from the ramped portion of the 200 mN tests (i.e. at  $\sim 310 \mu\text{m}$  scan distance – figure 7(b)) was compared to that from the constant load segments at 50 mN in figure 7(a). There was good agreement, with both approaches showing a reduction in friction coefficient over the first few cycles and levelling out thereafter. The “single point during load ramp” approach was then used to investigate the load dependence in a 200 mN test in figure 7(b). The friction coefficient increased slightly with load. The friction vs. cycles at different loads are shown in fig. 7(c). The variation in friction decreased with each cycle, most noticeably during the first few cycles. The corresponding on-load ( $h_t$ ), residual depth ( $h_r$ ) and scratch recovery data averaged over the entire constant load segment are shown in figure 7(d). The figure shows that (i)  $h_t$  and  $h_r$  increase cycle by cycle (ii) after the first few cycles

(where there is more ploughing and debris removal from the wear track) the SR approaches an approximately constant value of ~40 %.

The results from the last scratch and topography cycles for 3 repeat 41-pass tests at 200 mN are shown in Table 3. Surface profilometry measurements and SEM images (fig. 7(e)) showed that the initial surface topography had a periodic appearance from the grinding process, with alternate peaks and troughs and  $R_a \sim 60$  nm, decreasing to ~25 nm within a few scratch cycles and staying around this level until the end of the test (figure 7(f)). SEM imaging of the wear tracks (fig. 7(e)) confirmed the smoothing within the wear track. The variation in surface roughness under load was typically lower than in the subsequent topographic scan (fig. 7(g)).

#### 4.4 Noble metal alloy- noble metal alloy contacts

The mean friction and mean ECR per cycle are shown in figure 8 for (a) Ag-Ag (larger probe, 50 mN) (b,c) Ag-Ag 200 mN (d,e) Au-Au 200 mN. The mean friction coefficients and ECR over the first 500 and 5000 cycles in the longer tests are summarised in Table 4. Directionality was observed in contact resistance but was largely absent in the friction signal. In each test there were periodic dramatic increases in resistance which were accompanied by simultaneous rises in friction (e.g. after ~13500 and ~26000 cycles in the 200 mN test on Ag-Ag). Close examination of the event after ~13500 cycles is shown in figure 8(c) (confirms the change in friction). Aside from these events however, the friction and resistance were strongly *inversely* correlated. For the Au-Au there were two distinct types of resistance increase, either (i) approximately constant in forward and reverse directions or (ii) isolated failures occurring over a small portion of the sliding cycle, being more pronounced in one direction than the other. The first significant failure was preceded by a decrease in resistance and an increase in friction.

## 5. Discussion

### *5.1 Influence of surface topography and ploughing on friction evolution*

There is reasonable agreement between the friction coefficient (~0.2) measured in the low cycle repetitive scratch test and that in the initial stages of the reciprocating tests on the silver alloy. In the model proposed by Bowden and Tabor the total measured friction force can be considered to be the sum of the interfacial and ploughing terms (equation 3).

$$\mu = \mu_a + \mu_{pl} \quad [\text{Eqn. 3}]$$

where  $\mu_a$  = interfacial/adhesion component of the friction coefficient and  $\mu_{pl}$  = ploughing component. This 2-term equation has previously been used to explain the experimentally observed variation in friction with increasing number of cycles in the repetitive scratch test [9,26]. When the ploughing friction is sufficiently reduced by the repetitive cycling the measured friction has been taken as an estimate of the interfacial component [26]. The extent of quantitative correlation between the friction coefficient in the repetitive scratch and reciprocating wear tests to a large extent depends on the magnitude of the ploughing component in the tests, which is a function of the indenter geometry and applied load. The change in friction with load and cycles in the repetitive scratch test is consistent with changes in the ploughing term. The closeness of friction coefficients obtained from the ramped and constant load sections suggests a more efficient testing protocol than using only mean values from constant load segments in multi-cycle tests. For an instrument with sufficient lateral rigidity as the one used in this study, it is possible to obtain much more information from repetitive ramped scratches.

The initial cycles in the repetitive scratch test are dominated by changes due to wear altering the local surface topography within the scratch track. The variability in friction coefficient due to topographical variation along the scratch track decreased dramatically with each cycle. On smooth surfaces, it is possible to estimate the contact pressure in a repetitive scratch test by a Hertzian approach [27]. Applying this approach to the data in figure 7(d) results in an initial pressure of 2.7 GPa decreasing to 1.5 GPa after 20 cycles. The scratch width increased from 9.6 to 12.6  $\mu\text{m}$ . As shown by Korres et al [19], there is a correlation between track widening and the ploughing component to friction.

The initial decrease in friction in the reciprocating tests on 316L stainless steel, reducing ploughing friction through smoothing of surface asperities, was also observed in 10-cycle nano-scratch tests at 30 mN with a 3.7  $\mu\text{m}$  radius diamond [9] (data converted to friction coefficient in figure 9) and in 1 N tests on copper with a 100  $\mu\text{m}$  radius probe [26]. The higher friction measured in previous repetitive scratch tests with the smaller radius (3.7  $\mu\text{m}$ ) spheroconical probe are consistent with on-load scratch depths moving from the spherical to conical geometry.

The surface/near surface microstructure of the alloy may also evolve during sliding and influence the friction. With continued sliding grain refinement and/or formation of a tribologically transformed structure (TTS) has been reported for many alloys [14,21,26,28-32]. Suresh and co-workers have reported grain refinement resulting in an increase in hardness within the scratch track on Cu [26,30]. Cai and Bellon have shown that pin-on-disc wear tests of eutectic Ag-Cu (Ag-28.1wt.%Cu) resulted in grain refinement and work hardening within the wear track [31]. Laporte and co-workers used EDX measurements to show that a mechanically mixed layer (tribologically transformed structure) forms in multilayer sliding contacts with Ag top layers, with significant tribo-oxidation within the

wear track [14]. In the current work EDX maps of the wear tracks on the silver alloy revealed no oxidation within the track. EDX revealed Cu-rich regions of the unworn alloy. This structure was clearly visible by EDX in scratch tracks and in wear tracks from the reciprocating tests at 50 mN but in the 200 mN tracks there was some evidence of a TTS as the Cu distribution within the track was more uniform, indicating material movement and the formation of a more mechanically mixed layer.

A simplified single-term adhesion model for friction has previously been used to estimate the friction coefficient in clean, smooth, unlubricated noble metal contacts [33]. When ploughing is minimal, according to this model the friction force is the product of shear strength and the area of welded junctions between contacting asperities [34] (i.e. the force necessary to shear these junctions). The coefficient of friction is then expressed as the ratio of shear stress to normal stress. Assuming that the shear strength is approximately half of the yield strength,  $Y$ , and the contact pressure is  $\sim 3Y$  when asperities are in plastic deformation, results in an estimate of 0.17 for the friction coefficient. Notwithstanding the simplicity of this approach, when ploughing is minimised the measured friction coefficient was often close to this, being around 0.15-0.2 for the silver alloy for example.

### *5.2 Wear behaviour of 316L stainless steel and Ti6Al4V*

Marked differences between the alloys were observed. Stainless steel exhibited a ductile response throughout the load range. The friction force over a single cycle showed some variability due to the local surface topography which was more evident at the lowest load of 10 mN. Above 200 mN the wear depth increased more strongly with load than at lower load, and the friction reduction with cycling was more pronounced, consistent with a gradual change in attack angle as the probe geometry moves from the spherical end cap to the conical part. In contrast, an abrupt transition to higher friction and fracture-dominated wear after  $\sim 20$

cycles occurred at  $\geq 50$  mN on Ti6Al4V, resulting in higher final wear depth (figure 5(b)). The variation in the number of cycles to failure was expected due to the complex microstructure/local mechanical property variation in this alloy.

Nanoindentation tests with a Berkovich indenter at 100 mN, i.e. a sufficiently high load that the native surface oxide (1.9 nm for 316L stainless steel [35] and 4-5 nm for Ti6Al4V [36-37]) does not affect the results, have shown that Ti6Al4V is somewhat harder but lower in elastic modulus than the 316L stainless steel. This combination of mechanical properties results in higher elastic strain to break ( $H/E$ ) and resistance to plastic deformation,  $H^3/E^2$ . At lower load wear appears to be controlled by its mechanical properties, resulting in more elastic deformation and lower wear depth than 316L stainless steel.

EDX oxygen mapping across the 316L and Ti6Al4V wear tracks provide information on the nature of the TTS formed in the 500 cycle tests. On Ti6Al4V the amount of oxygen enrichment in the wear track was strongly load-dependent. For the tests at 20-40 mN there was no enrichment in the wear track (so EDX maps were completely featureless), slight enrichment at 50 mN and more significant oxygen from 70 mN. The changes in friction with continued cycling were accompanied by roughening of the wear track. To illustrate this figure 10 (a,b) shows how the surface profile over the central part of the wear track changes from near the start (a = cycle 2) to the end (b = cycle 499) at 20 mN (i.e. below the transition, so little roughening). In comparison, friction and surface profiles from a test at 100 mN are shown in figure 10 (c-e) for cycles 6, 20 and 250 (before/after the transition). In contrast on the 316L stainless steel there was no oxygen enrichment in the wear track at 100 mN and only very slight enhancement at the edges of the track at 200 and 500 mN.

We have previously investigated the tribologically transformed structures that form after reciprocating wear of 316L stainless steel and Ti6Al4V using FIB-imaging, EDX [21] and

nanomechanical measurements [32]. There are clear differences between the TTS on these biomaterials. On Ti6Al4V the TTS is much thicker and EDX shows it is accompanied by significant surface oxidation whereas on 316L it is much thinner and tribo-oxidation revealed by EDX is much less. It was shown that these structures form rapidly and initially increase hardness on both materials. After further wear cycles on Ti6Al4V there was a transition to a softer and less stiff TTS that is more porous [21,32].

The EDX measurements in the current study are in good agreement with the previous work [21] and provide further support for the influence of the TTS on the measured friction. When the native oxide is still present in the wear track it protects the underlying alloy enabling a hard, low friction TTS to form. With continued cycling at higher load the depth increases on Ti6Al4V there is a transition from the spherical end cap to the conical part of the tip increasing the attack angle which can influence the dominant deformation. Several authors have reported a transition from ploughing wear to cutting as the attack angle increases [38]. On Ti6Al4V this more severe contact results in break-up of the protective oxide leading to (i) much higher friction (ii) increase in oxygen (iii) rougher and more porous surface with reduction in mechanical properties.

The friction and wear evolution in the Ti6Al4V tests has some parallels with what has been observed previously in nano-fretting (gross slip) and nano-scratch (unidirectional) tests on this alloy [39]. Abrupt transitions with load were observed in reciprocating nano-wear (nano-fretting) tests (diamond,  $R = 3.7 \mu\text{m}$  end radius, 3000 cycles over  $10 \mu\text{m}$  track length at 10 Hz). At 1-3 mN there was minimal wear but there was a transition to severe wear from 4 mN. In repetitive nano-scratch tests at 30 mN with the same probe the friction and wear rate remained high with continued scratch cycles, and were accompanied by a large decrease in scratch recovery, consistent with less effective formation of a protective, load-supporting

TTS (in comparison to 316L stainless steel and CoCrMo where the wear rate and friction rapidly reduce and the reduction in scratch recovery is much less, indicating formation of a protective TTS). SEM images of repetitive nano-scratch tracks reveal similarities with the higher load reciprocating tests, with non-smooth profile within the track (i.e. indicative of cold-welding/adhesive stick-slip) consistent with the highly variable scratch depth along it [39].

Complex microstructure and susceptibility to brittle deformation makes wear difficult to predict in Ti6Al4V tribosystems [40-43]. Several factors appear responsible for the tribological behaviour on the Ti6Al4V with marked transition to more severe wear as the load increases. It has a harder surface oxide [44] which effectively protects the underlying alloy at low load. Removal of the hard oxide layer with increasing cycling at higher load exposes the Ti alloy surface. In fretting-wear studies its wear rate is typically an order of magnitude higher than 316L stainless steel despite the much lower hardness of the steel [21,32]. Molinari and co-workers have noted that the surface oxide which forms in dry sliding of Ti6Al4V can be very thick but oxygen tends to embrittle the matrix reducing its mechanical strength [42]. Li et al noted that the tribolayers on Ti6Al4V were relatively porous with a high number of cracks [43]. Dong and Bell reported that in pin-on-disc tests wear of an alumina ball sliding against Ti6Al4V was three orders of magnitude higher than when sliding against hardened steel [41]. Break-up of the weak surface oxide on the titanium surface was considered responsible.

In contrast, in the current tests on 316L stainless steel the oxide is intact through the load range, resulting in ploughing and low friction. Under these conditions a hard, thin TTS can develop with continued cycling. Pile-up is more significant in sliding contact than indentation and is also influenced by  $H/E$  and  $a/R$  (where  $a$  is the contact radius and  $R$  is the indenter radius) [45-46]. There is more pile-up on 316L stainless steel due to its lower  $H/E$ .

### 5.3 Combining friction and ECR in reciprocating sliding in noble metal contacts

A very low number of cycles to failure accompanied by a rapid rise in friction is typical of unlubricated electroplated Au sliding [33]. Tian and co-workers reported a multi-stage deformation in sphere-on-flat reciprocating sliding tests between electroplated gold contacts (Au-Ni vs Au-Ni) on brass substrate [10]:- (i) in stage I sliding was Au-Au with removal of the gold layer was associated with a significant rise in friction to  $\mu \sim 0.8$  after about 90 cycles (ii) sliding was Au-Nickel in stage II with  $\mu$  decreasing to  $\sim 0.4-0.5$  and (iii) from  $\sim 200$  cycles sliding was Au-brass in stage III with  $\mu$  increasing to  $\sim 0.6-1.2$  and becoming more variable. A similarly low number of cycles to failure and multi-stage process were also observed on the connector studied in this work. The observed variability in the time-to-failure being most likely related to differences in local surface roughness (at  $\sim 100$  nm, the  $R_a$  was  $>$  thickness of the electroplated gold layer). Liskiewicz and co-workers have recently shown that surface roughness can exert a strong influence on the endurance of electrical connectors for automotive applications in fretting tests [47].

There are distinct benefits of combining ECR and friction measurements as they may be able to provide complementary information. Differing reports in the literature exist regarding the level of correlation between the two measurements. Prasad and co-workers reported an inverse correlation between the coefficient of friction and the electrical contact resistance for copper contacts in the mild wear regime ( $0.2 < \mu \leq 0.4$ ) [48]. High contact resistance for  $\mu < 0.2$  was considered to be due to an oxide layer at the interface. Tamai [49], Tian [10] reported a complete lack of correlation between friction and the electrical contact resistance. In these studies there was little or no change in contact resistance [10] or friction [49] to sliding wear whilst the other parameter was sensitive to it. Tamai argued that increasing resistance due to oxide debris may not alter the friction if the debris strongly adheres to the sliding surfaces

and does not change the shear strength. Tian et al stated that contact resistance is not a good indicator of the sliding failure of electroplated contacts in laboratory tests [10] but the results in this current work do not support this as a general conclusion.

There were notable differences between the behaviour of the noble metal alloy systems and the electroplated multilayer thin film, most obviously that the number of sliding cycles required for failure of the bulk alloy was much larger than for the thin film interconnector system. In contrast to the multilayer films sliding against the nominally axisymmetric steel ball, the Au and Ag alloys sliding against connector pins with more complex (non-axisymmetric) geometries showed marked directionality in the contact resistance once failure was initiated. The mean value of the electrical contact resistance over a single cycle loses this directional information but provides a convenient measure of changing behaviour with the number of cycles.

The tests shown in fig. 8 have revealed a complex relationship between friction and electrical contact resistance. For the alloy systems, the friction and contact resistance generally decrease over the first few cycles [figure 11 (a,b)]. The decrease in contact resistance is consistent with the asperities on the probe and disk being smoothed out which increases the contact area. The decrease in friction occurs due to a reduction in ploughing, with a possible contribution from grain refinement [31]. ECR is higher for the tests with the larger probe at lower load as it is more difficult to flatten asperities so this is less efficient and takes longer. Correlation between the friction and ECR, when both increase dramatically and subsequently recover, is likely to be largely topographic in nature, with non-conducting non-noble metal oxide debris trapped in the contact increasing the contact area. In the 35000 cycle Ag alloy-Ag alloy test the two obvious increases in friction and resistance (after 13500 and 26000 cycles) may relate to oxide debris being trapped in contact that eventually is removed from the sliding contact. The inverse correlation observed otherwise may be related to changing

metallic/non-metallic composition of the contact, e.g. where the metallic contact area is decreasing this could be due to more (previously buried) oxide fragments in the contact, as suggested by Prasad and co-workers in the reciprocating wear of copper sliding contacts [48]. The general behaviour on the Au-Au was similar with a decrease in resistance and increase in friction preceding the first isolated failure of the Au-Au couple suggestive of an increase in metallic contact area.

## **6. Conclusions**

The stability to perform long duration reciprocating tests, including a 35000 cycle (46 hr) test, has been demonstrated. Integrating the capability for high cycle, long duration reciprocating nano-/micro-scale tests into a commercial instrument extends the versatility of the multi-functional test instrumentation. In reciprocating tests noble metal-noble metal contacts (Au-Au and Ag-Ag) showed much longer endurance than gold vs. steel contacts. Improved detection of the onset of wear and the subsequent failure mechanisms was possible by simultaneously monitoring friction and ECR. Changes in electrical contact resistance showed a complex correlation with changes to the measured friction, through changes in the electrically conductive contact area.

In reciprocating nano-wear tests with diamond probes the biomedical alloys Ti6Al4V and 316L stainless steel showed markedly difference behaviour as a function of applied load. Stainless steel exhibited a ductile response throughout the load range. At higher loads on Ti6Al4V there was an abrupt transition to higher friction and fracture-dominated wear after ~20 cycles, as illustrated by the data in figures 4 and 5.

The repetitive ramped scratch approach tested here has the potential to provide significantly more data on the evolution of the friction with cycling than the constant load repetitive scratch test.

### **Acknowledgements**

This work was supported by the Engineering and Physical Sciences Research Council (EPSRC), Grant No. ELP01629X and Micro Materials Ltd. as part of the EPSRC Doctoral Training Centre in Integrated Tribology (iT-CDT).

### **References**

1. K. Meine, T. Schneider, D. Spaltmann, E. Santner, The influence of roughness on friction Part I. The influence of a single step, *Wear* 253 (2002) 725-732.
2. K. Meine, T. Schneider, D. Spaltmann, E. Santner, The influence of roughness on friction Part II. The influence of multiple steps, *Wear* 253 (2002) 733-738.
3. D. Drees, J.-P. Celis, S. Achanta, Friction of thin coatings on three length scales under reciprocating sliding, *Surf. Coat. Technol.* 188-189 (2004) 511-518.
4. S. Achanta, D. Drees, J.-P. Celis, Friction and nanowear of hard coatings in reciprocating sliding at milli-Newton loads, *Wear* 259 (2005) 719-729.
5. E. Santner, D. Klaffke, K. Meine, C. Polaczyk, D. Spaltmann, Demonstration of topography modification by friction processes and vice versa, *Tribol. Int.* 39 (2006) 450-455.
6. E. Santner, D. Klaffke, K. Meine, C. Polaczyk, D. Spaltmann, Effects of friction on topography and vice versa, *Wear* 261 (2006) 101-106.

7. S. Achanta, D. Drees, J.-P. Celis, Friction from nano to macroforce scales analysed by single and multiple-asperity contact approaches, *Surf. Coat. Technol.* 202 (2008) 6127-6135.
8. K. Holmberg, A. Laukkanen, H. Ronkainen, R. Waudby, G. Stachowiak, M. Wolski et al, Topographical orientation effects on friction and wear in sliding DLC and steel contacts, part 1: Experimental, *Wear* 330-331 (2015) 3-22.
9. B.D. Beake, A.J. Harris and T.W. Liskiewicz, Review of recent progress in nanoscratch testing, *Tribology* 7 (2013) 87.
10. H. Tian, N. Saka, E. Rabinowicz, Friction and failure of electroplated sliding contacts, *Wear* 142 (1991) 57-85.
11. T. Liskiewicz, S. Fouvry, Development of a friction energy capacity approach to predict the surface coating endurance under complex oscillating sliding conditions, *Tribol. Int.* 38 (2005) 69-79.
12. T. Liskiewicz, S. Fouvry, B. Wendler, Development of a Wöhler-like approach to quantify the Ti(CxNy) coatings durability under oscillating sliding conditions, *Wear* 259 (2005) 835-841.
13. R. Rybiak, S. Fouvry, T. Liskiewicz, B. Wendler, Fretting wear of a TiN PVD coating under variable relative humidity conditions – development of a ‘composite’ wear law, *Surf. Coat. Technol.* 202 (2008) 1753-1763.
14. J. Laporte, O. Perrinet, S. Fouvry, Prediction of the electrical contact endurance of silver-plated coatings subject to fretting wear, using a friction energy density approach, *Wear* 330-331 (2015) 170-181.
15. S. Fouvry, J. Laporte, O. Perrinet, P. Jedrzejczyk, O. Graton, Fretting wear of low current electrical contacts: quantification of electrical endurance, *IEEE Holm Conference on Electrical Contacts*, 2017.

16. F.G. Echeverrigaray, S.R.S de Mello, L.M. Leidens, C.D. Boeira, A.F. Michels, I. Braceras, C.A. Figueroa, Electrical contact resistance and tribological behaviors of self-lubricated dielectric coating under different conditions, *Tribol. Int.* 143 (2020) 106086.
17. A. Kassman, S. Jacobson, Surface damage, adhesion and contact resistance of silver plated copper contacts subjected to fretting motion, *Wear* 165 (1993) 227-230.
18. D.L. Burris, W.G. Sawyer, Addressing Practical Challenges of Low Friction Coefficient Measurements, *Tribol. Lett.* 35 (2009) 17-23.
19. S. Korres, T. Feser, M. Dienwiebel, A new approach to link the friction coefficient with topography measurements during plowing, *Wear* 303 (2013) 202-210.
20. T.J. Kamps, J.C. Walker, A.G. Plint, In-situ stylus profilometer for high frequency reciprocating tribometer. 2017 *Surf. Topogr.: Metrol. Prop.* 5 034004.
21. Y. Liu, T.W. Liskiewicz, B.D. Beake, Dynamic changes of mechanical properties induced by friction in the Archard wear model, *Wear* 428-429 (2019) 366-375.
22. B. Shi, J.L. Sullivan and B.D. Beake, An investigation into which factors control the nanotribological behaviour of thin sputtered carbon films, *J Phys D: Appl Phys* 41 (2008) 045303.
23. G.M. Wilson, J.F. Smith, J.L. Sullivan, A nanotribological study of thin amorphous C and Cr doped amorphous C coatings, *Wear* 265 (2008) 1633-1641.
24. G.M. Wilson, "An investigation of thin amorphous carbon-based sputtered coatings for MEMS and Micro-engineering applications", PhD Thesis, Aston University, June 2008.
25. J.A. Williams, H.R. Le, Tribology and MEMS, *J.Phys.D: Appl.Phys.* 39 (2006) R201–R214.

26. T. Hanlon, A.H. Chokshi, M. Manoharan, S. Suresh, Effects of grain refinement and strength on friction and damage evolution under repeated sliding contact in nanostructured metals, *Int. J. Fatigue* 27 (2005) 1159-1163.
27. B.D. Beake, S.R. Goodes and B. Shi, Nanomechanical and nanotribological testing of ultra-thin carbon-based and MoST films for increased MEMS durability, *J Phys D: Appl Phys* 42 (2009) 065301.
28. E. Sauger, L. Ponsonnet, J.M. Martin, L. Vincent, Study of the tribologically transformed structure created during fretting tests, *Tribol. Int.* 33 (2000) 743-750.
29. E. Sauger, S. Fouvry, L. Ponsonnet, Ph. Kapsa, J.M. Martin, L. Vincent, Tribologically transformed structure in fretting, *Wear* 245 (2000) 39-52.
30. A. Singh, M. Dao, L. Lu, S. Suresh, Deformation, structural changes and damage evolution in nanotwinned copper under repeated frictional contact sliding, *Acta Mater.* 59 (2011) 7311-7324.
31. W. Cai, P. Bellon, Subsurface microstructure evolution and deformation mechanism of Ag-Cu eutectic alloy after dry sliding wear, *Wear* 303 (2013) 602-610.
32. T. Liskiewicz, K. Kubiak, T. Comyn, Nano-indentation mapping of fretting-induced surface layers, *Tribol. Int.* 108 (2017) 186-193.
33. N. Aukland, H. Hardee, P. Lees, Sliding wear experiments on clad gold-nickel material systems lubricated with a 6-ring polyphenyl ether, *Proc. 46th IEEE Holm Conf. Elect. Contacts*, 2000, 27-35.
34. R.W. Wilson, The contact resistance and mechanical properties of surface films on metals, *Proc. Phys. Soc. B* 68 (1955) 625-641.
35. S. Tardio, M.-L. Abel, R.H. Carr, J.E. Castle and J.F. Watts, A Comparative Study of the Native Oxide on 316L Stainless Steel by XPS and ToF-SIMS, *JVST A* 33, (2015) 05E122.

36. B.W. Callen, B.F. Lowenberg, S. Lugowski, R.N.S. Sodhi, and J.E. Davies, Nitric acid passivation of Ti6Al4V reduces thickness of surface oxide layer and increases trace element release, *J. Biomed. Mater. Res.* 29 (1995) 279-290.
37. C. Sittig, M. Textor, N. D. Spencer, M. Wieland, P.-H. Vallotton, Surface characterization of implant materials c.p. Ti, Ti-6Al-7Nb and Ti-6Al-4V with different pretreatments, *J. Mater. Sci.: Mater. In Medicine* 10 (1999) 35-46.
38. K.I. Schiffmann, Microtribological/mechanical testing in 0, 1 and 2 dimensions: A comparative study on different materials, *Wear* 265 (2008) 1826-1836.
39. B.D. Beake and T.W. Liskiewicz, Comparison of nano-fretting and nano-scratch tests on biomedical materials, *Tribol. Int.* 63 (2013) 123-131.
40. F. Zivic, M. Babic, S. Mitrovic, A. Vencl, Continuous control as alternative route for wear monitoring by measuring penetration depth during linear reciprocating sliding of Ti6Al4V alloy, *J. Alloys Cmpd.* 509 (2011) 5748-5754.
41. H. Dong and T. Bell, Tribological behaviour of alumina sliding against Ti6Al4V in unlubricated contact, *Wear* 225-229 (1999) 874-884.
42. A. Molinari, G. Straffelini, B. Tesi, T. Bacci, Dry sliding wear mechanisms of the Ti6Al4V alloy, *Wear* 208 (1997) 105-112.
43. X.X. Li, Q.Y. Zhang, Y. Zhou, J.Q. Liu, K.M. Chen, S.Q. Wang, Mild and Severe Wear of Titanium Alloys, *Tribol. Lett.* 61 (2016) 14.
44. N. Moharrami, D.J. Langton, O. Sayginer, S.J. Bull, Why does titanium alloy wear cobalt chrome alloy despite lower bulk hardness: A nanoindentation study? *Thin Solid Films* 549 (2013) 79-86.
45. B. Taljat and G.M. Pharr, Development of pile-up during spherical indentation of elastic-plastic solids, *Int. J. Sol. Struct.* 41 (2004) 3891-3904.

46. S.C. Bellemare, M. Dao, S. Suresh, Effects of mechanical properties and surface friction on elasto-plastic sliding contact. *Mech. Mater.* 40 (2008) 206-219.
47. T.W. Liskiewicz, K.J. Kubiak, D.L. Mann, T.G. Mathia, Analysis of surface roughness morphology with TRIZ methodology in automotive electrical contacts: Design against third body fretting-corrosion, *Tribol. Int.* 143 (2020) 106019.
48. V.S. Prasad, P. Misra, J. Nagaraju, An experimental study to show the behaviour of electrical contact resistance and coefficient of friction at low current sliding electrical interfaces, 57th Holm Conference on Electrical Contacts (Holm), IEEE 2011. <https://doi.org/10.1109/HOLM.2011.6034813>.
49. Y. Tamai, The friction and contact resistance of metals and alloys in a reciprocating sliding, *ASLE Transactions* 3 (1960) 26-29.

## Tables

**Table 1 Typical test conditions in various NanoTest Vantage microtribological tests**

	Nano-scratch	Nano-fretting	NanoTriboTest
Motion	Unidirectional	Reciprocating	Reciprocating
Sliding speed (mm/s)	0.001-0.1	0.01	1-10
Track length (mm)	0.01-1	0.02	1-10
Number of cycles	1-20	1000-200000	100-30000
Total sliding distance (m)	0.00001-0.01	0.01-0.1	1-300
Probe radius ( $\mu\text{m}$ )	5-25	10-200	25-5000

**Table 2 Conditions in reciprocating nano-wear tests vs. metallic probes**

Sample	Probe	Load (mN)	Track length (mm)	Set I (A)	Cycles	Time (s)	Sliding distance (mm)
Au multilayer	Steel	10	5	0.1	~200	1000	2000
Ag alloy	Ag alloy	50	10	0.5	1221	5746	24420
Au alloy	Au alloy	200	5	0.5	11532	54908	115320
Ag alloy	Ag alloy	200	5	0.1	35000	166482	350000

**Table 3 On-load and residual depths after 20 cycles at 200 mN\***

	$h_t$ ( $\mu\text{m}$ )	$h_r$ ( $\mu\text{m}$ )	SR
Test #1	$1.58 \pm 0.17$	$0.92 \pm 0.21$	41.4
Test #2	$1.42 \pm 0.14$	$0.98 \pm 0.15$	30.9
Test #3	$1.45 \pm 0.23$	$0.83 \pm 0.25$	42.6

\* Scratch recovery (SR) was determined from the on-load depth ( $h_t$ ) and residual depth ( $h_r$ ).

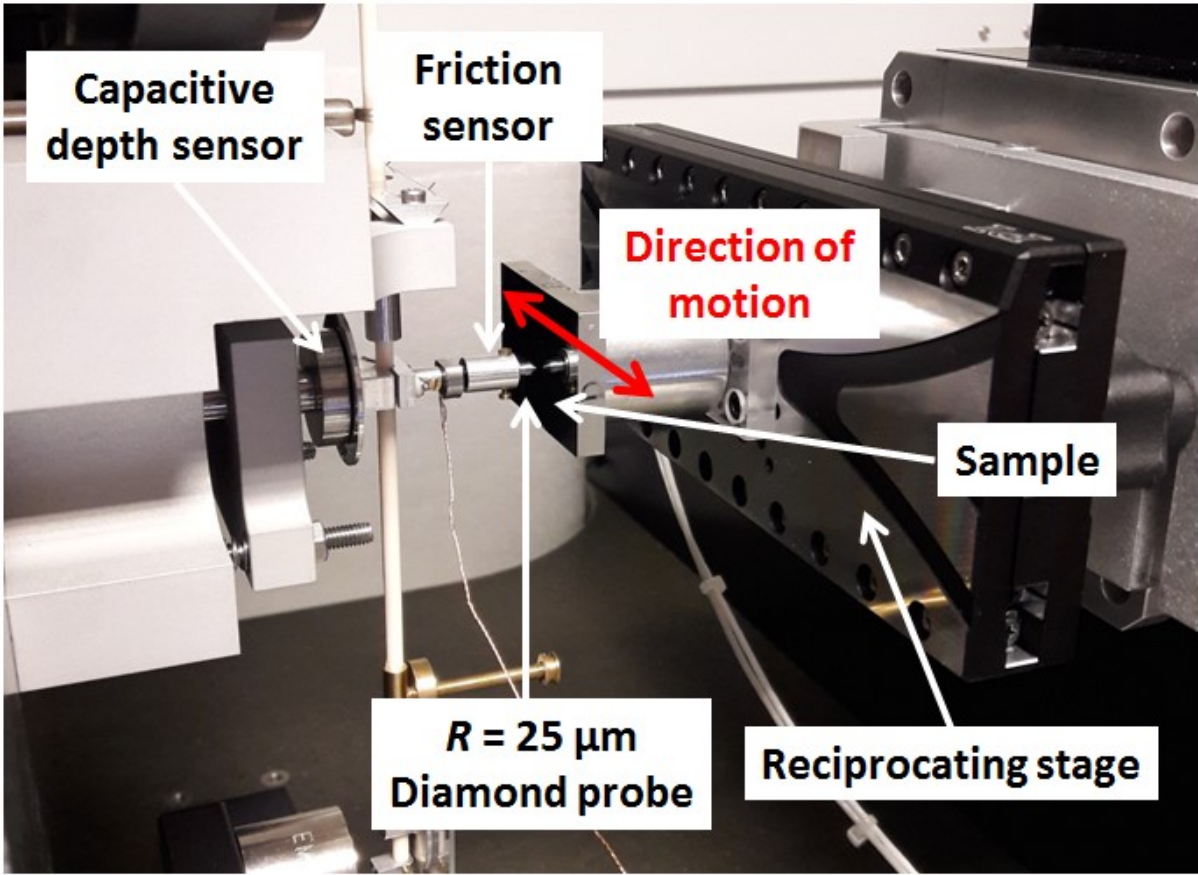
Mean and standard deviation data are taken over the entire track distance scanned at peak load i.e. from 250-1000  $\mu\text{m}$ .

**Table 4 Mean friction coefficient and ECR over 500 and 5000 cycles in noble metal alloy contacts**

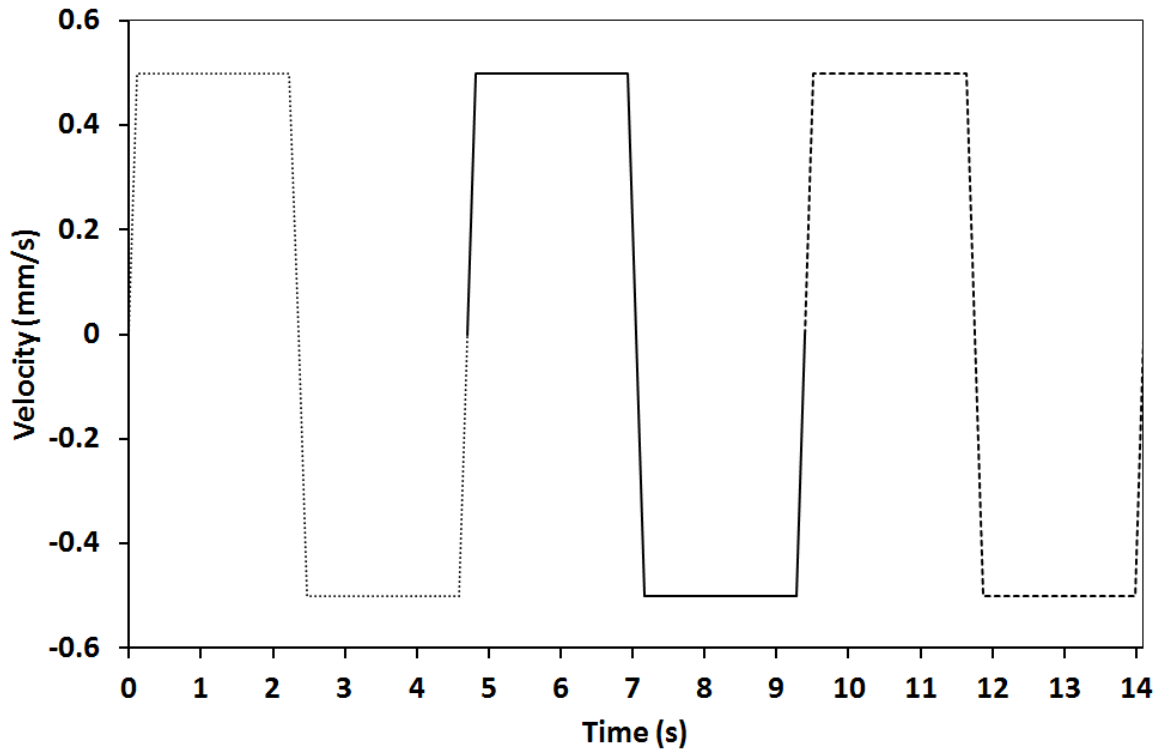
	Ag-Ag, 50 mN	Ag-Ag, 200 mN		Au-Au, 200 mN	
	500 cycles	500 cycles	5000 cycles	500 cycles	5000 cycles
Friction coefficient	$0.14 \pm 0.03$	$0.21 \pm 0.03$	$0.15 \pm 0.02$	$0.09 \pm 0.01$	$0.09 \pm 0.02$
ECR ( $\Omega$ )	$0.09 \pm 0.08$	$0.03 \pm 0.03$	$0.14 \pm 0.12$	$0.01 \pm 0.00$	$0.02 \pm 0.01$

## Figure captions

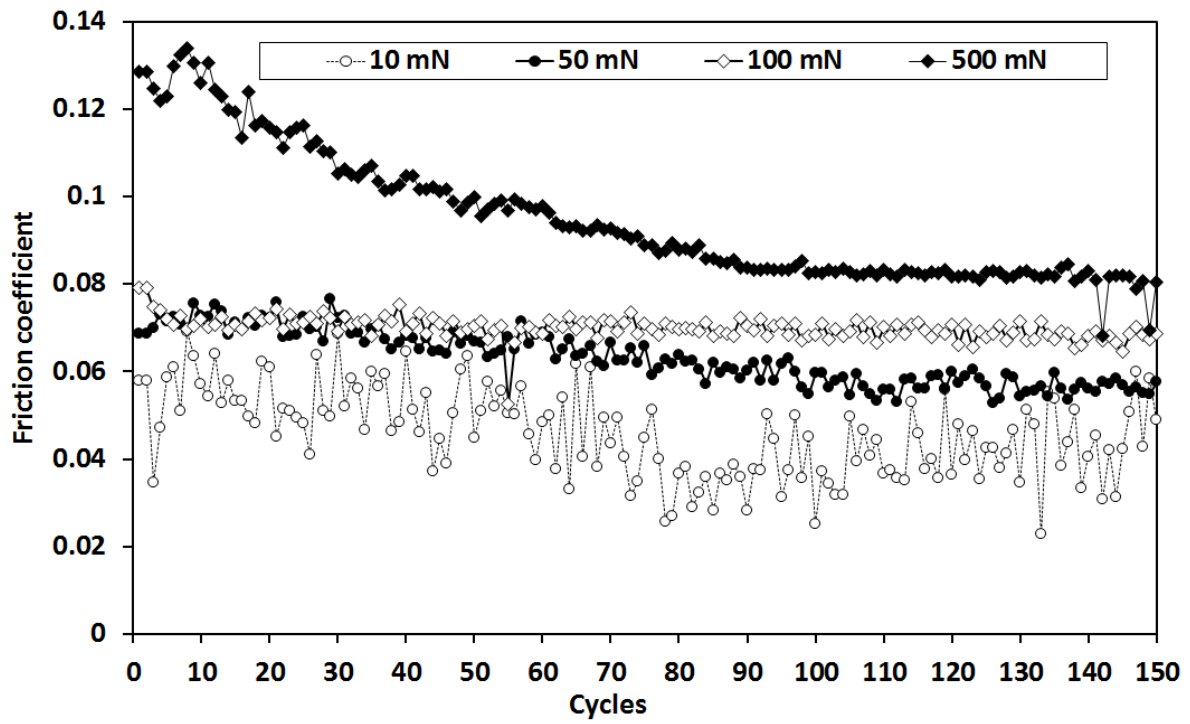
1. (a) Experimental setup for reciprocating wear with PI stage (b) Illustrative velocity vs. time profile in a reciprocating test, showing 3 cycles at 0.5 mm/s velocity and 5 s trace-retrace cycle duration.
2. Reciprocating tests on 316L stainless steel. (a) Friction coefficient vs. cycles at 10-500 mN (b) on-load wear depth vs. cycles. (c) SEM images of the wear tracks (d) high magnification image of 500 mN track.
3. Reciprocating tests on Ti6Al4V. (a) An example test at 100 mN example showing transition (b) friction loops before (closed squares), just after the transition (closed triangles) and at the mid-point (open circles) of the 500 cycle test. (c) Energy dissipation vs. cycles (d) cumulative energy dissipation vs. cycles.
4. SEM images of wear tracks on Ti6Al4V at (a) 30 mN (b) 40 mN (c) 50 mN (d) 70 mN (e, f) 100 mN.
5. (a) Friction coefficient vs. cycles on 316 L stainless steel and Ti6Al4V at 30 and 50 mN (b) Final wear depth at 50-500 mN on 316 L stainless steel and Ti6Al4V.
6. Reciprocating tests on electroplated gold. (a-d) friction and ECR for 4 time segments (a) 280-350 mm sliding distance; 133-166 s; (b) 350-420 mm sliding distance; 166-199 s; 420-490 mm sliding distance; 199-232 s; d 910-980 mm sliding distance; 432-465 s. (e) Mean  $\mu$  and ECR vs. cycles in a typical test and (f) corresponding non-averaged ECR (g) ECR vs. cycles from 6 repeat tests.
7. Nano-scratch. (a) friction coefficient vs. cycles at 50 mN (b) Load history repetitive scratch at 200 mN (c) friction coefficient vs. load for 1,5,10,20 cycles (d) depth and scratch recovery in repetitive scratch at 200 mN (e) SEM image of 200 mN scratches (f) variation in topography for pre-scan and after scratches 1-5. Data offset in y-axis for clarity (pre-scan is lowest y, scratch 5 is highest) (g) comparison of on-load and topographic profile for #5,#6.
8. Mean friction and mean resistance per cycle (a) Ag-Ag (larger probe, 50 mN) (b) Ag-Ag 200 mN (c) Ag-Ag 200 mN; event after ~13500 cycles (d) Au-Au. (e) 0-5000 cycles on Au-Au. (full red circles = friction coefficient; open blue circles = ECR).
9. Friction coefficient vs. cycles in repetitive nano-scratch testing of Ti6Al4V and 316L stainless steel with 3.7  $\mu\text{m}$  end radius diamond probe.
10. Friction and surface profile correlations. Ti6Al4V at 20 mN, (a) = after 2 cycles, (b) = after 499 cycles. Ti6Al4V at 100 mN, (c) = after 6 cycles, (d) = after 20 cycles, (e) = after 250 cycles.
11. Friction (a) and resistance (b) decrease over the first 50 cycles in noble metal-noble metal contacts.



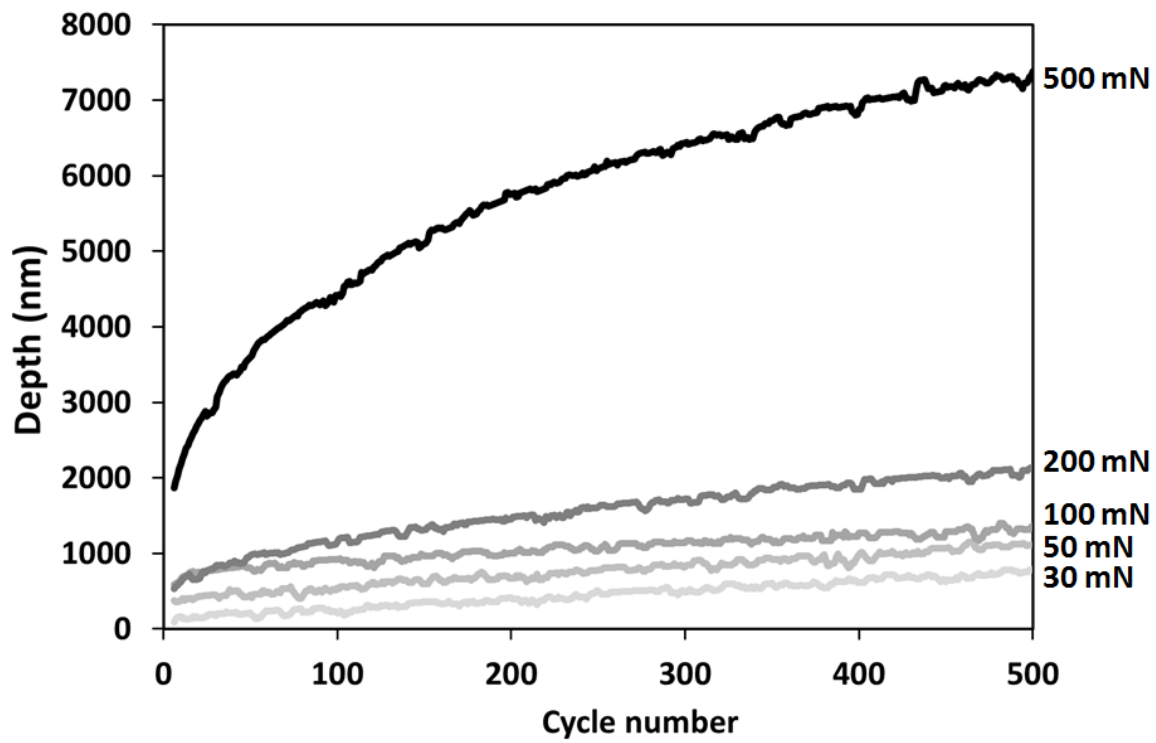
1(a)



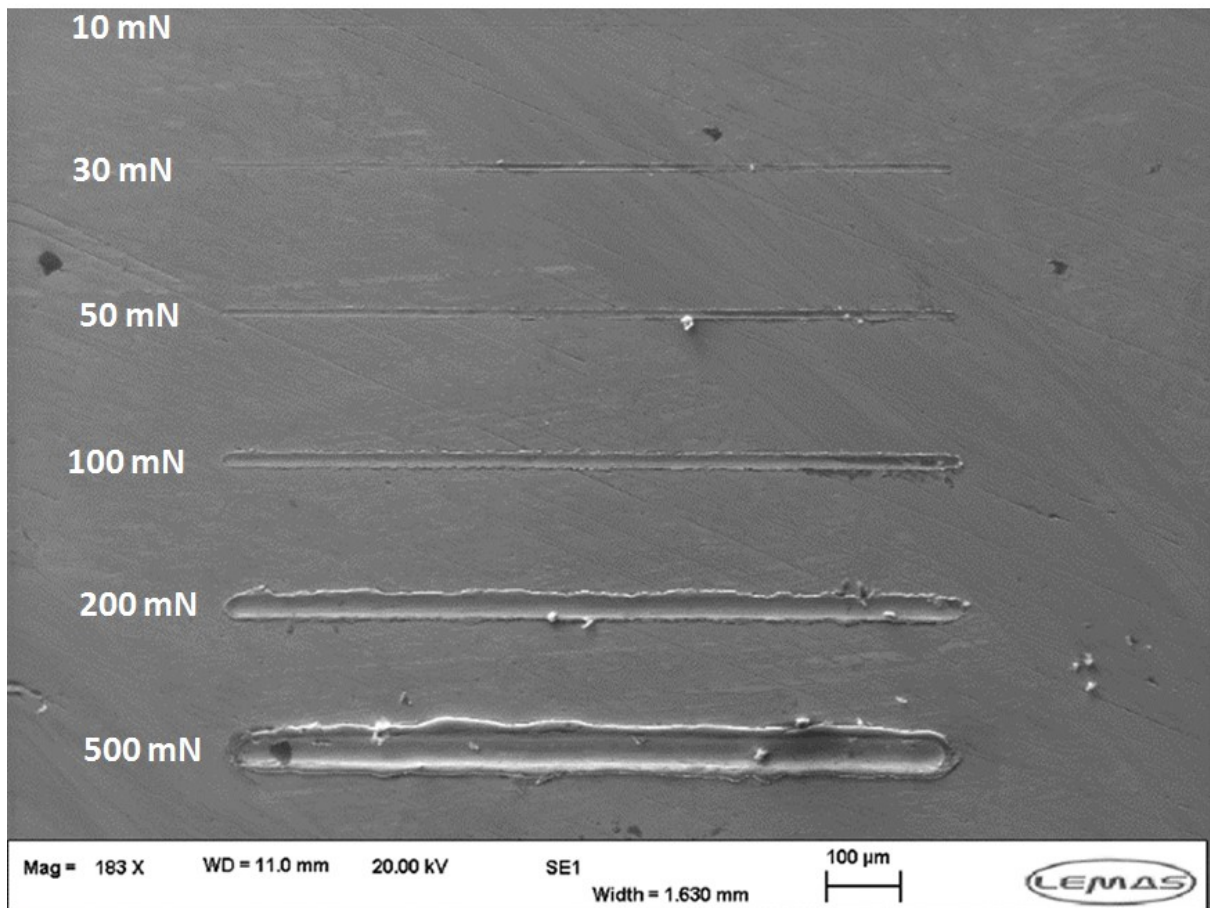
1(b)



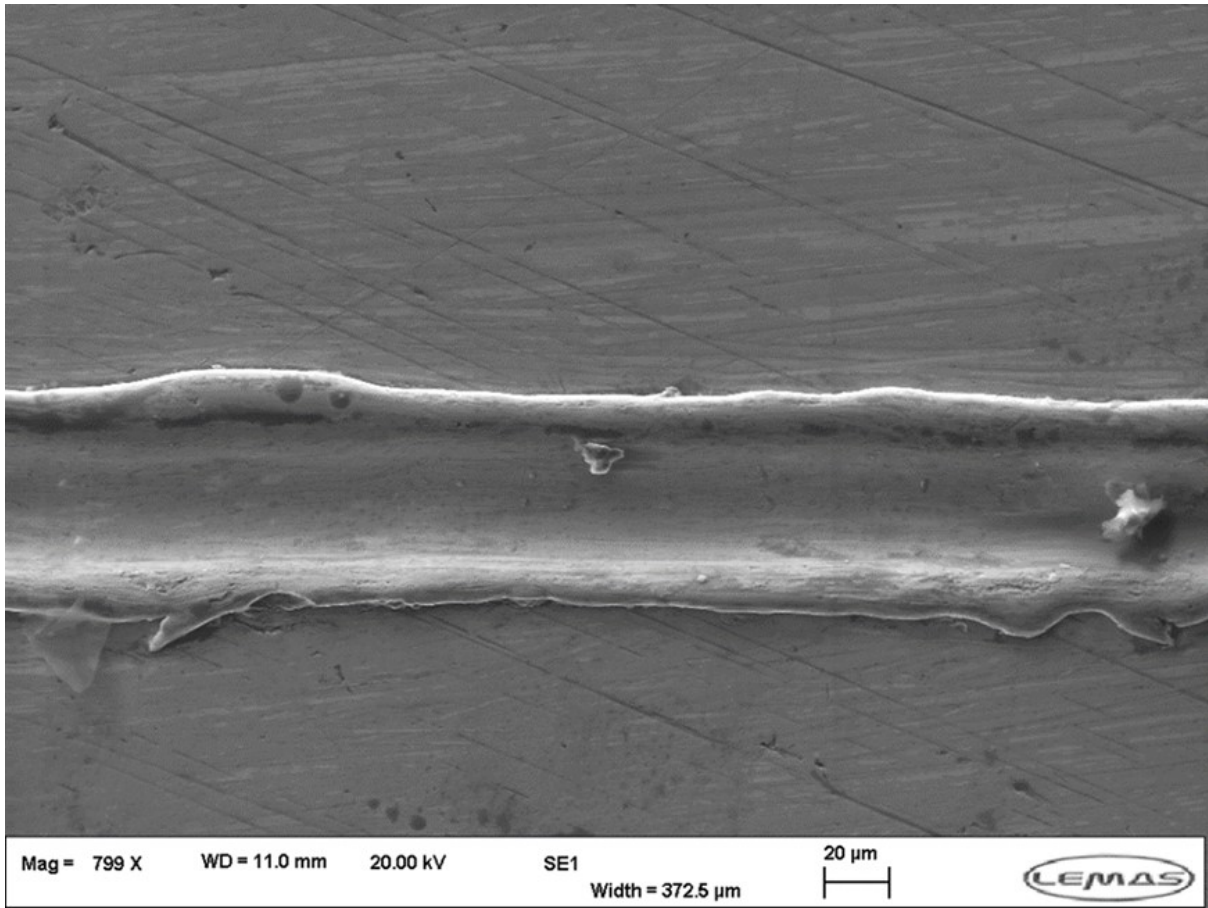
2(a)



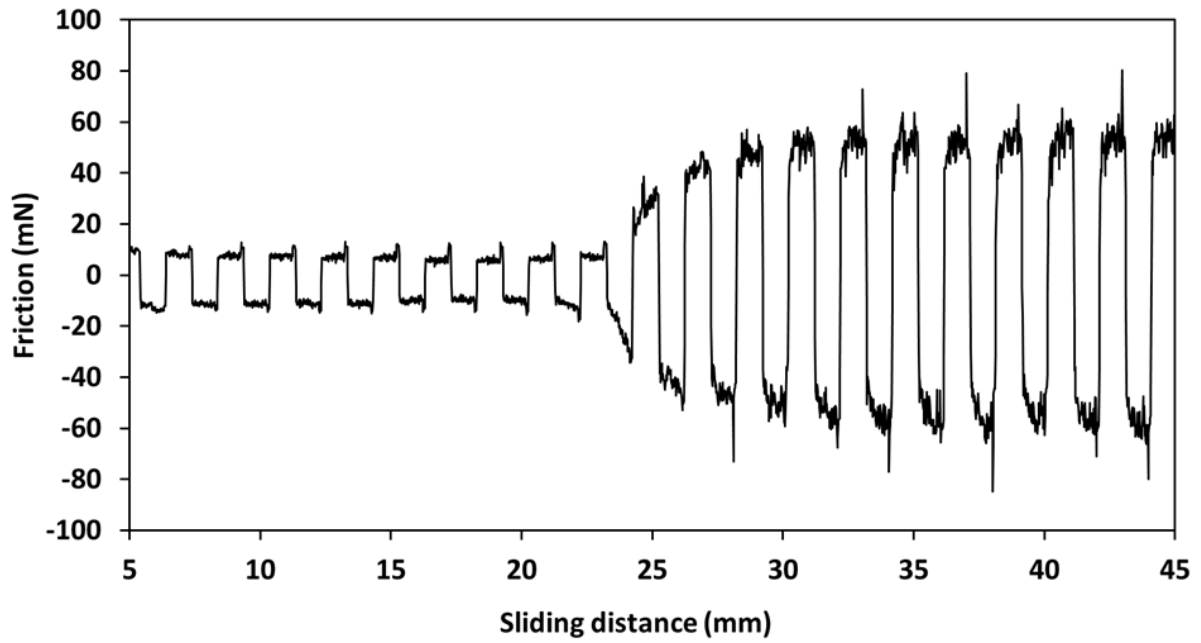
2 (b)



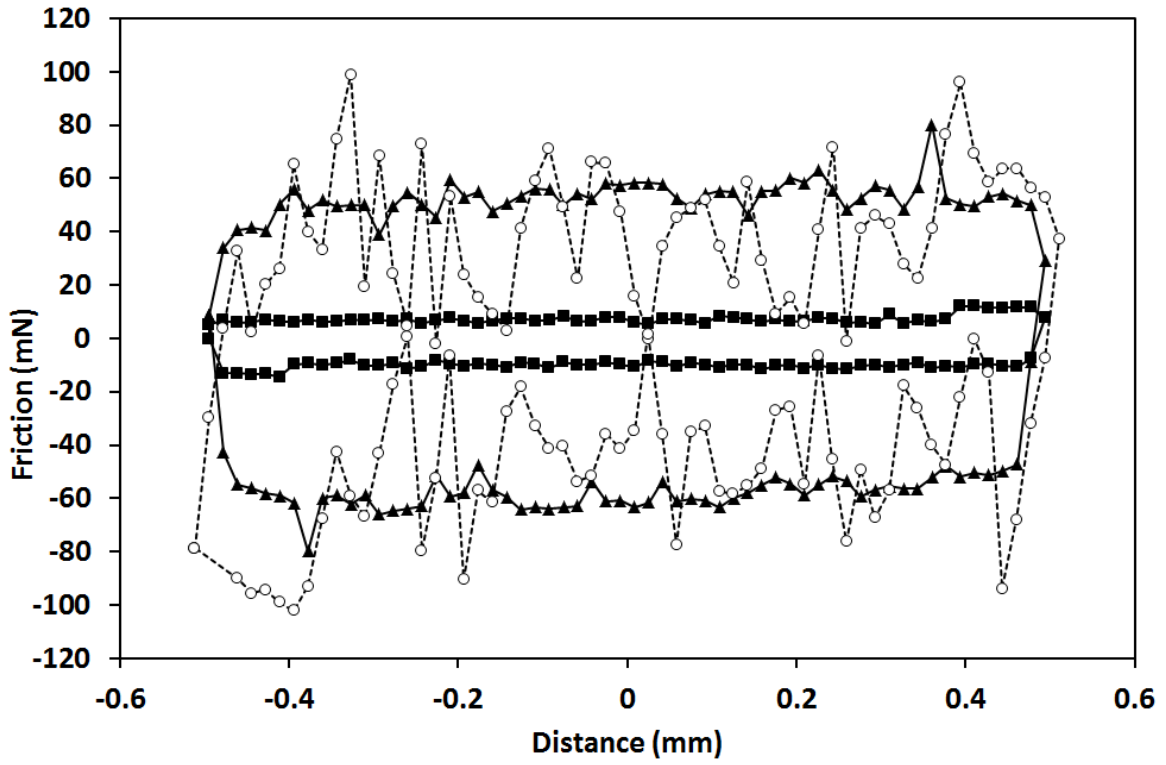
2 (c)



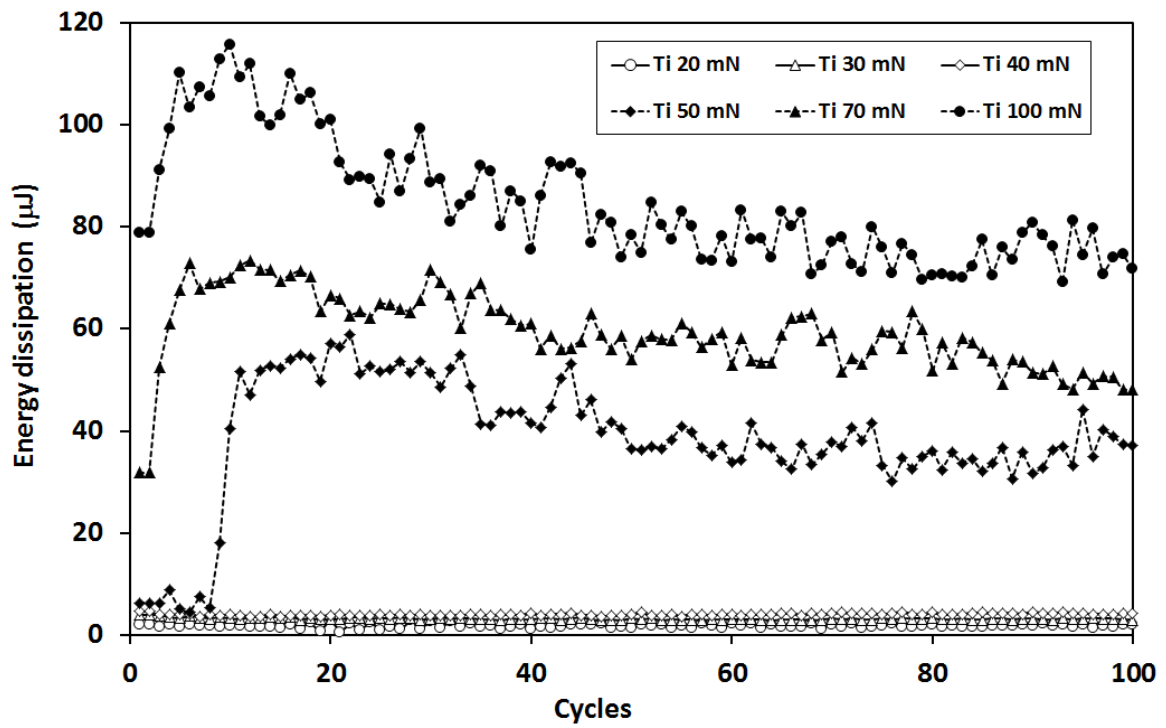
2(d)



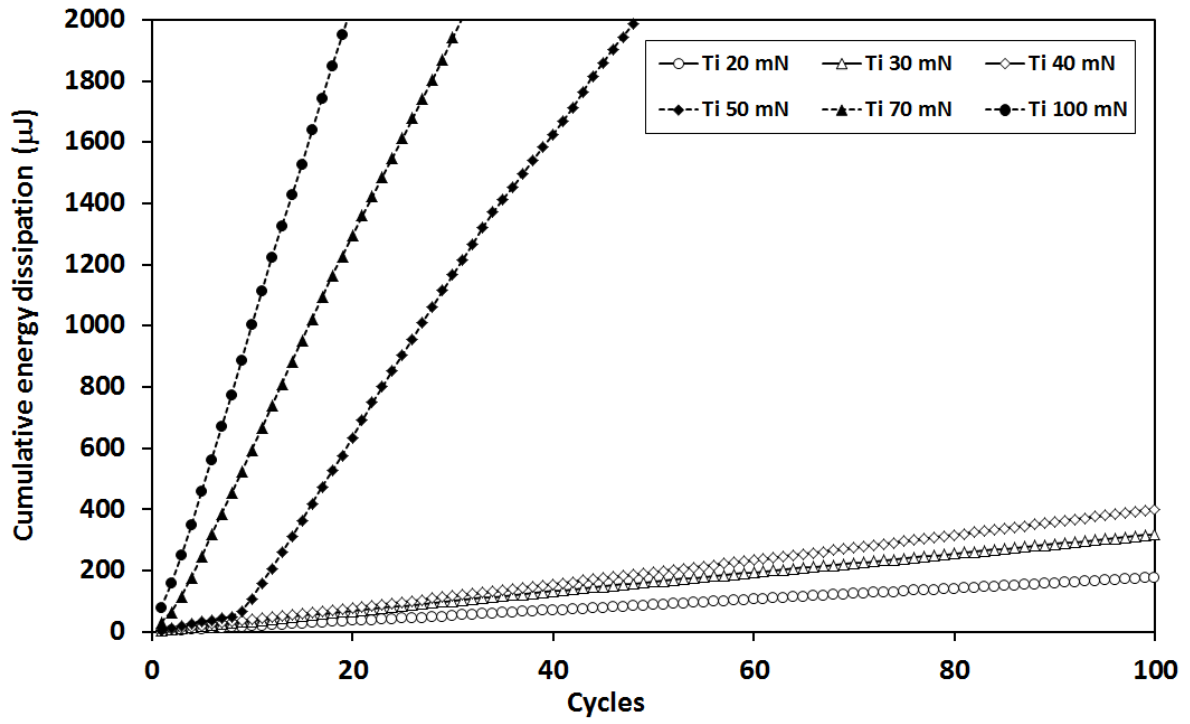
3(a)



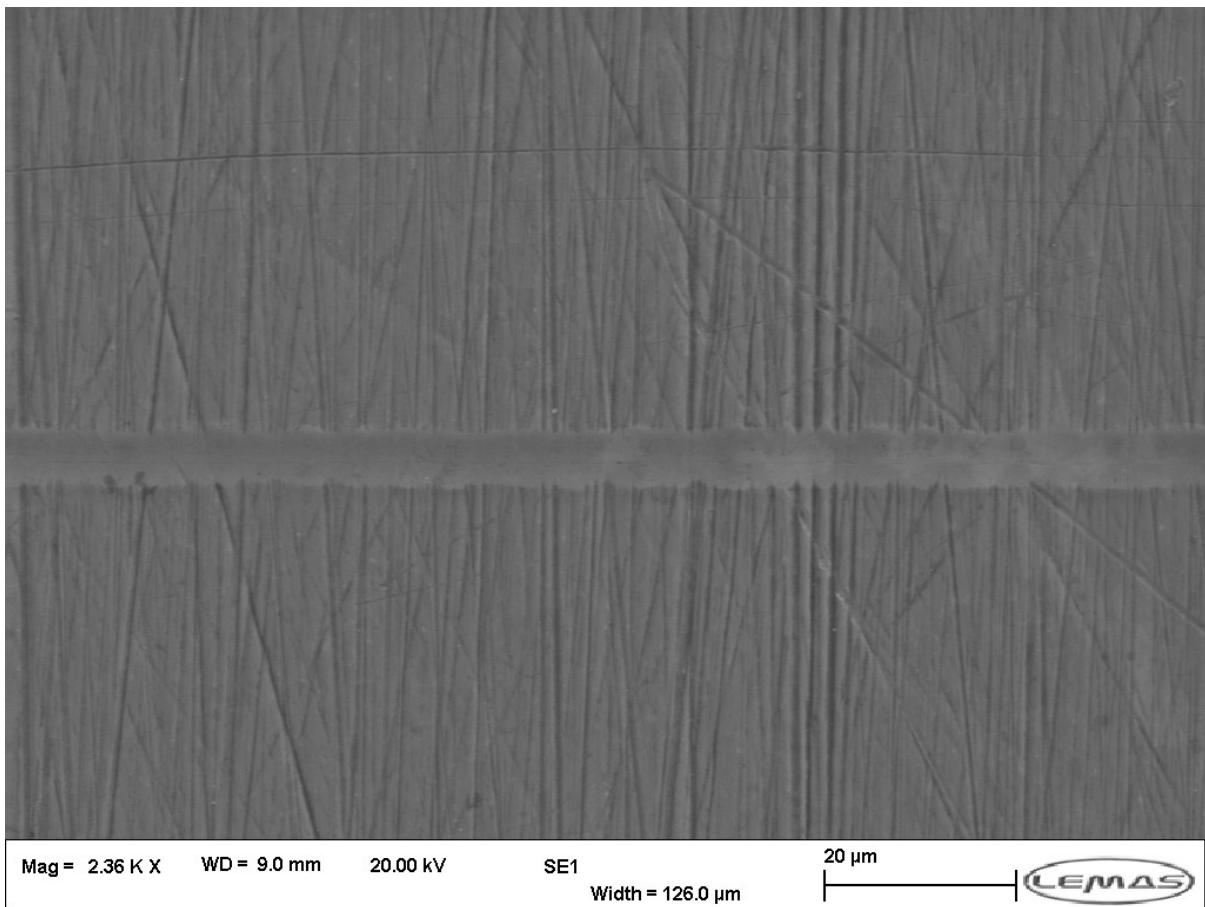
3(b)



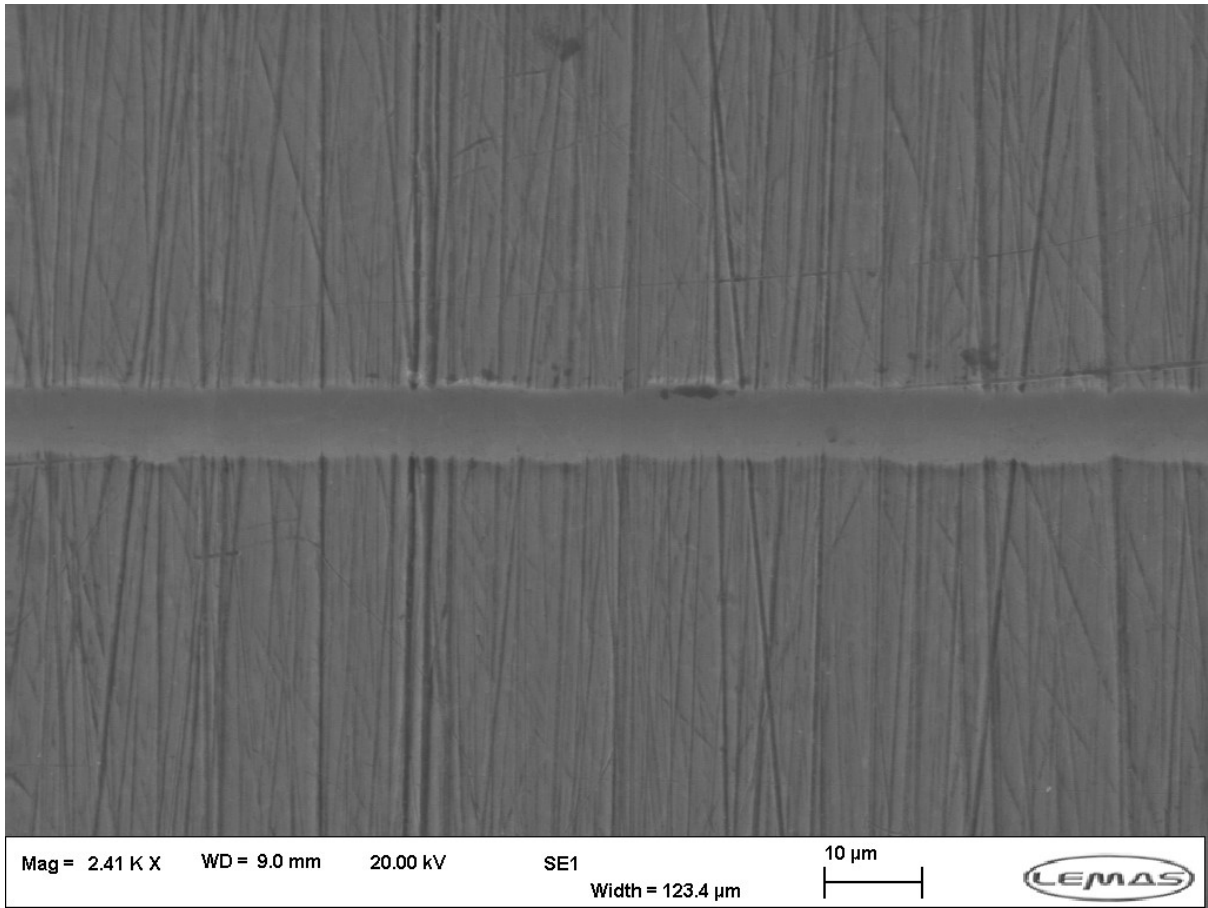
3(c)



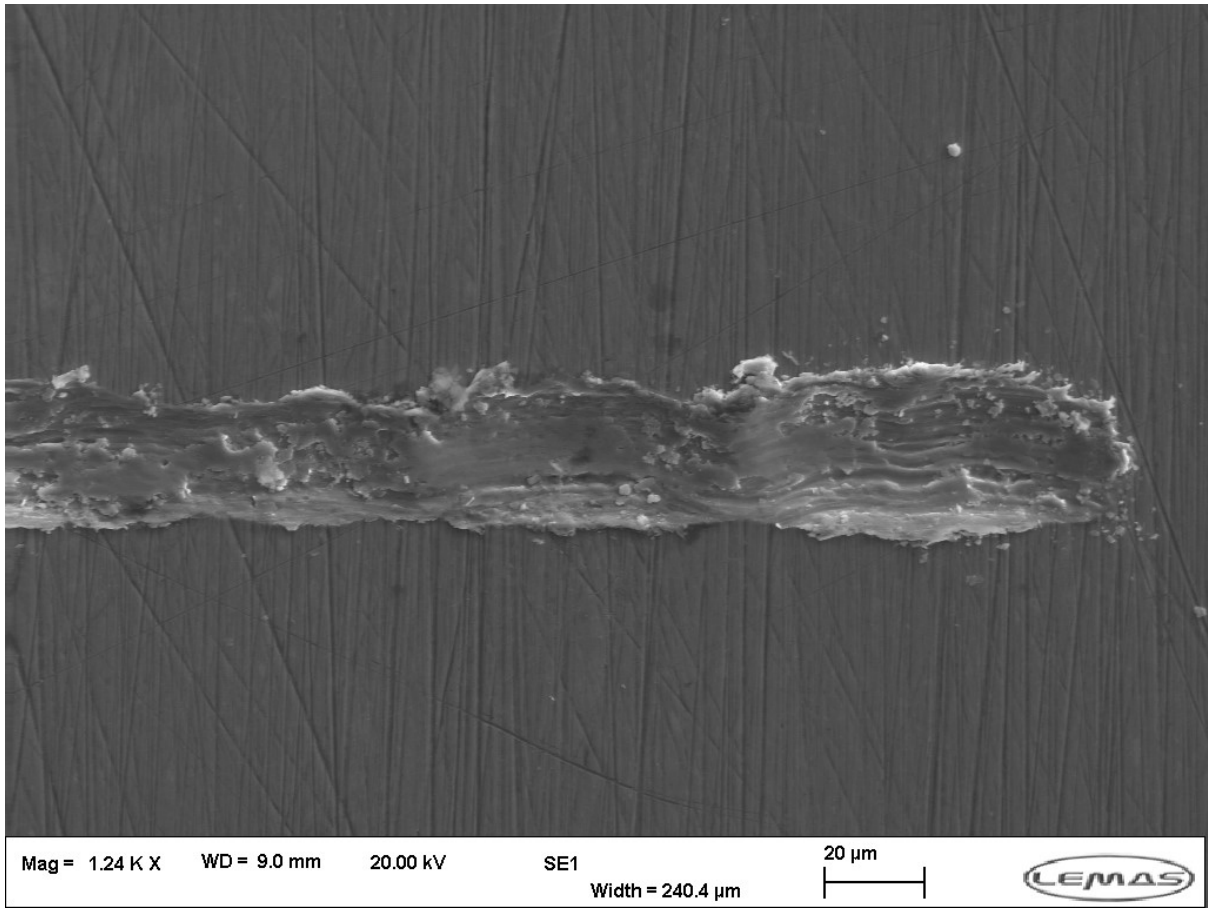
3(d)



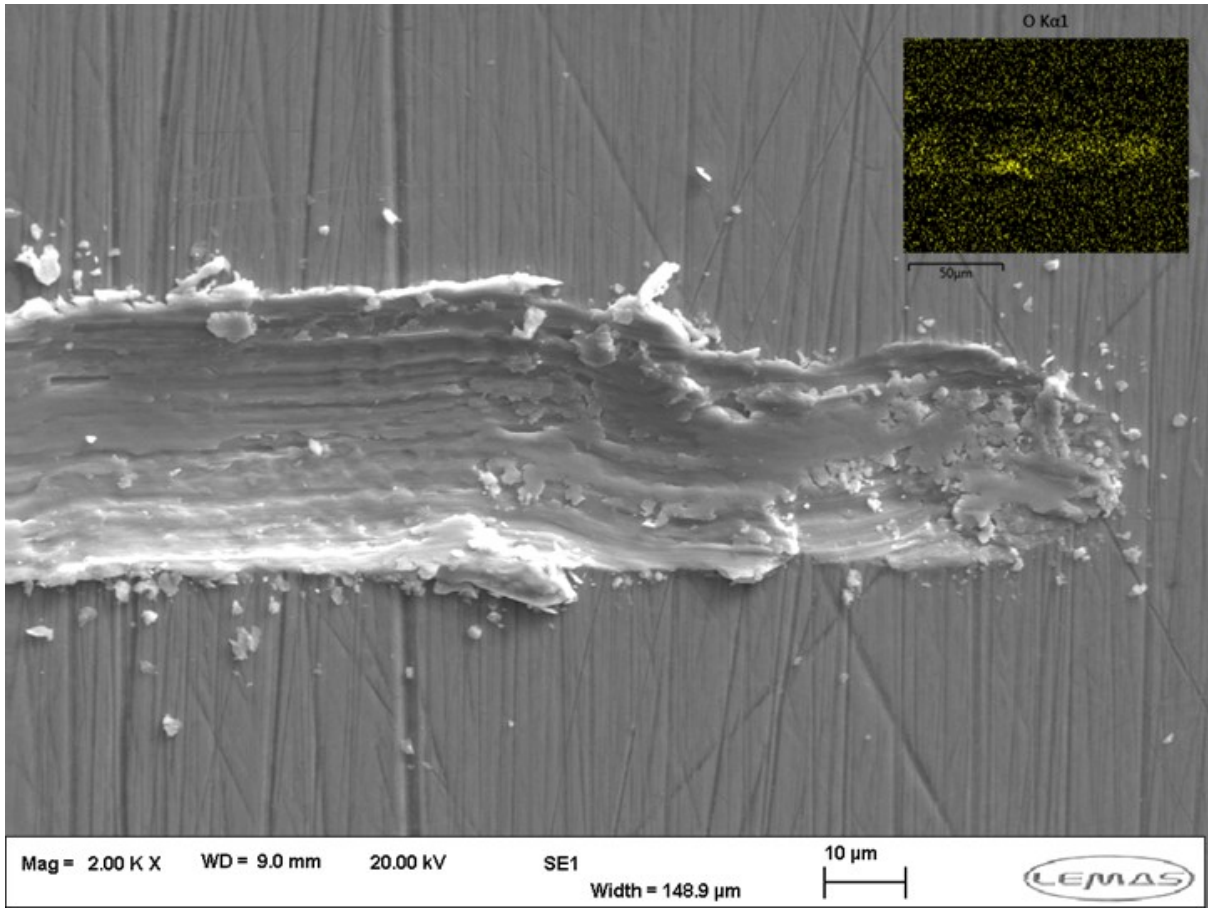
4(a)



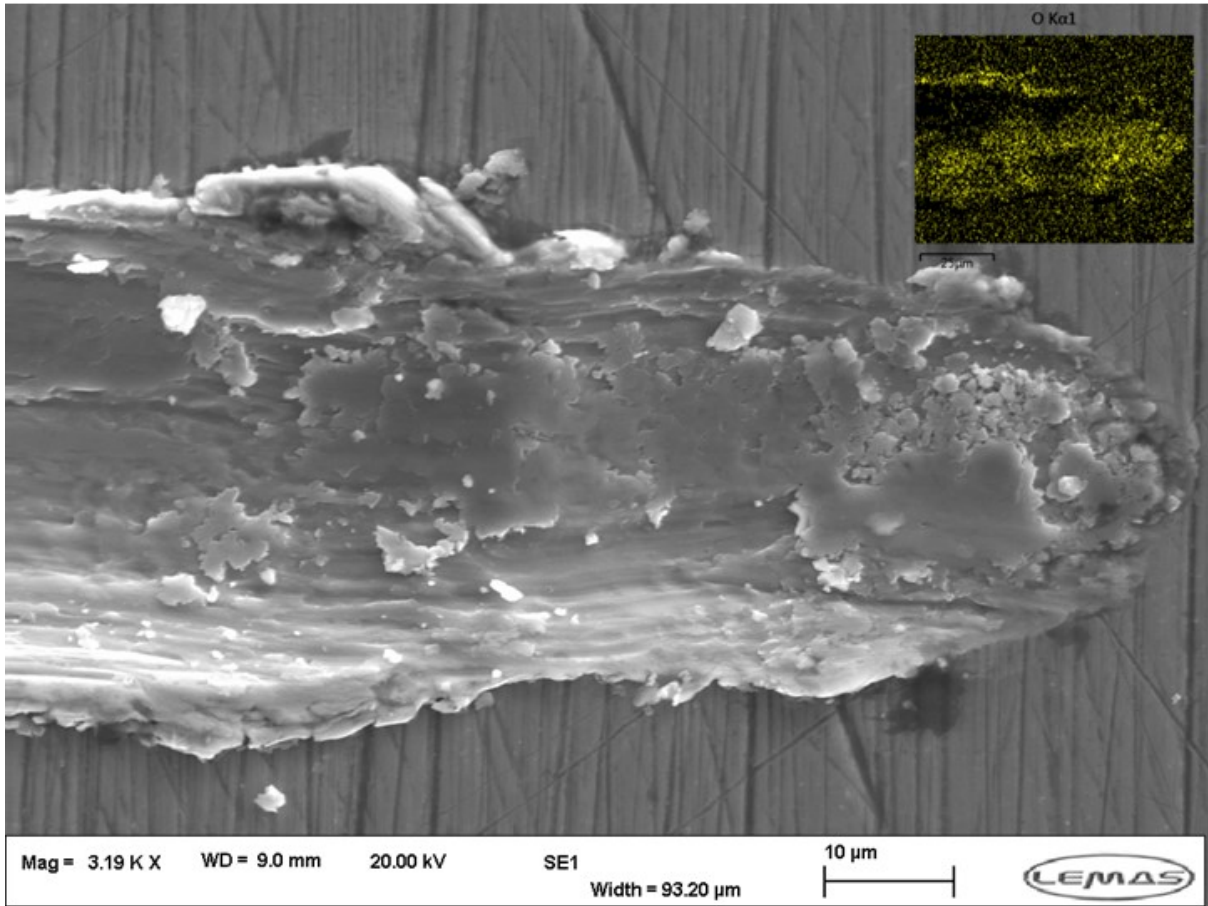
4(b)



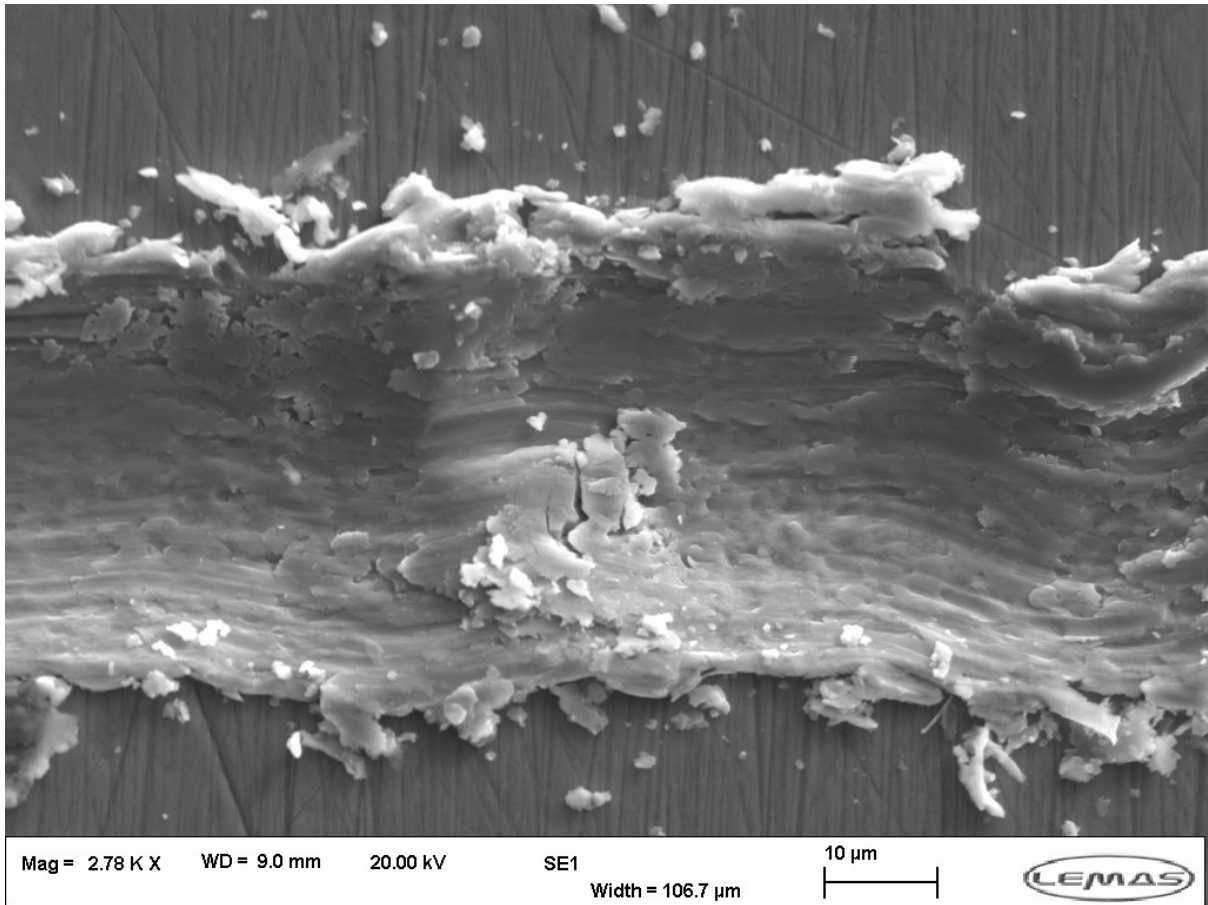
4 (c)



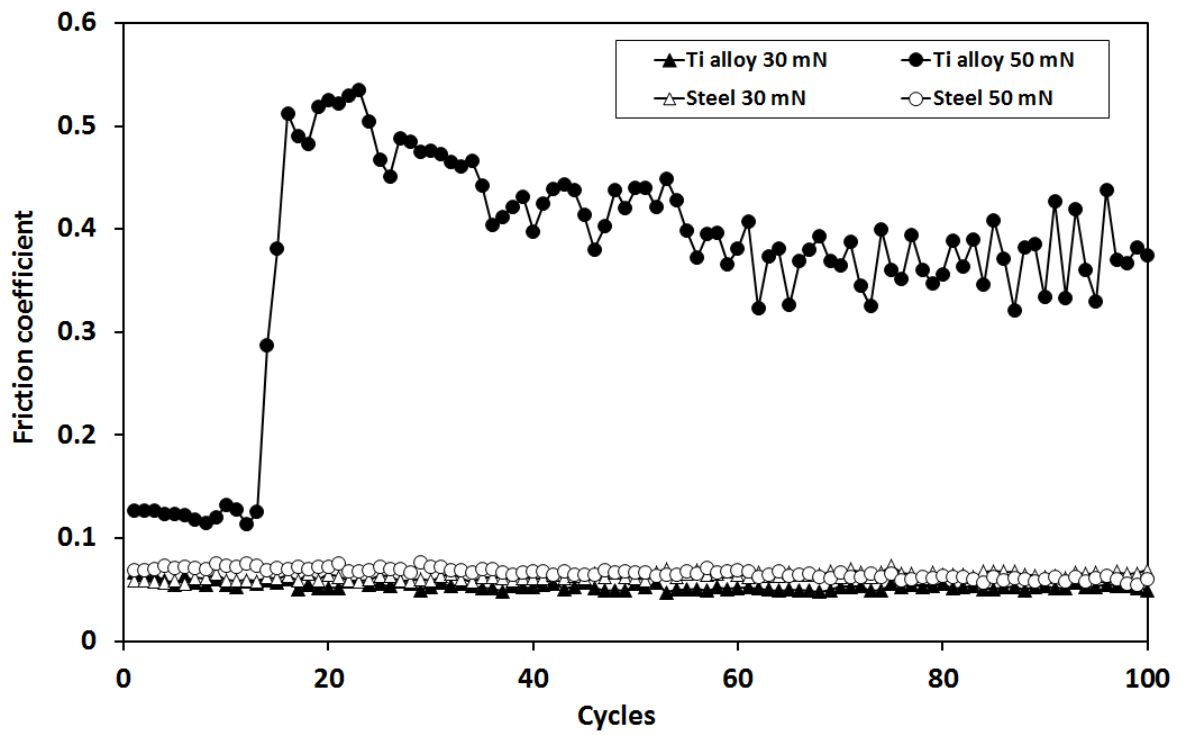
4 (d)



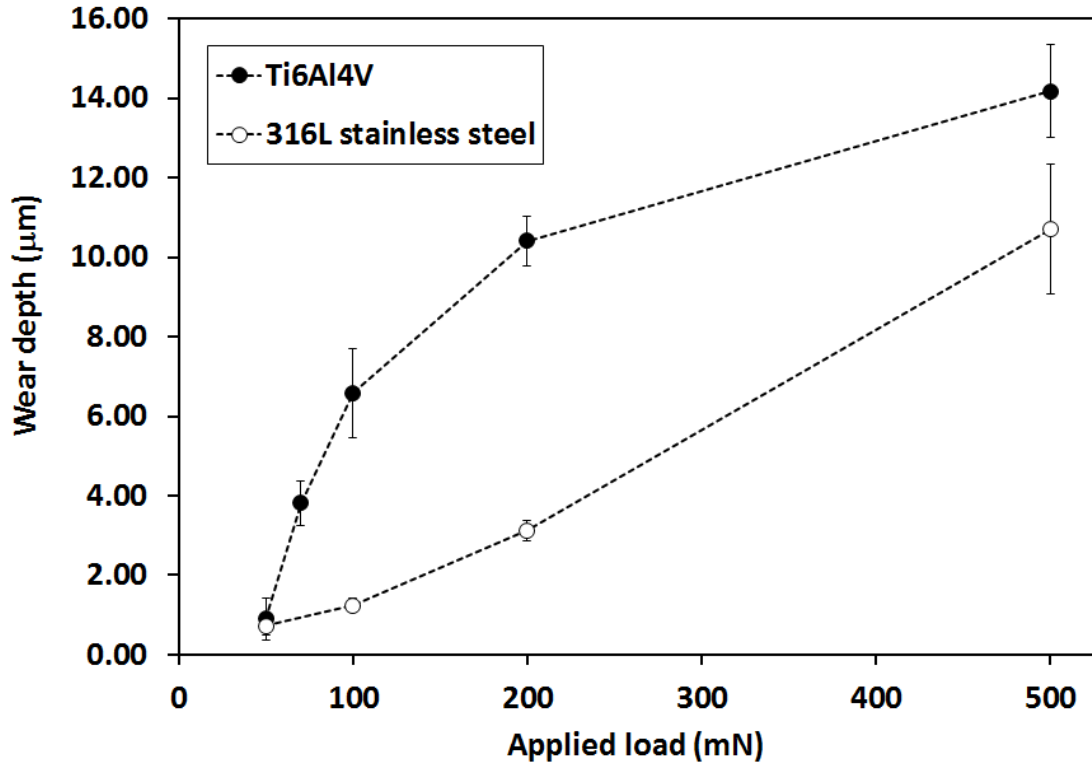
4(e)



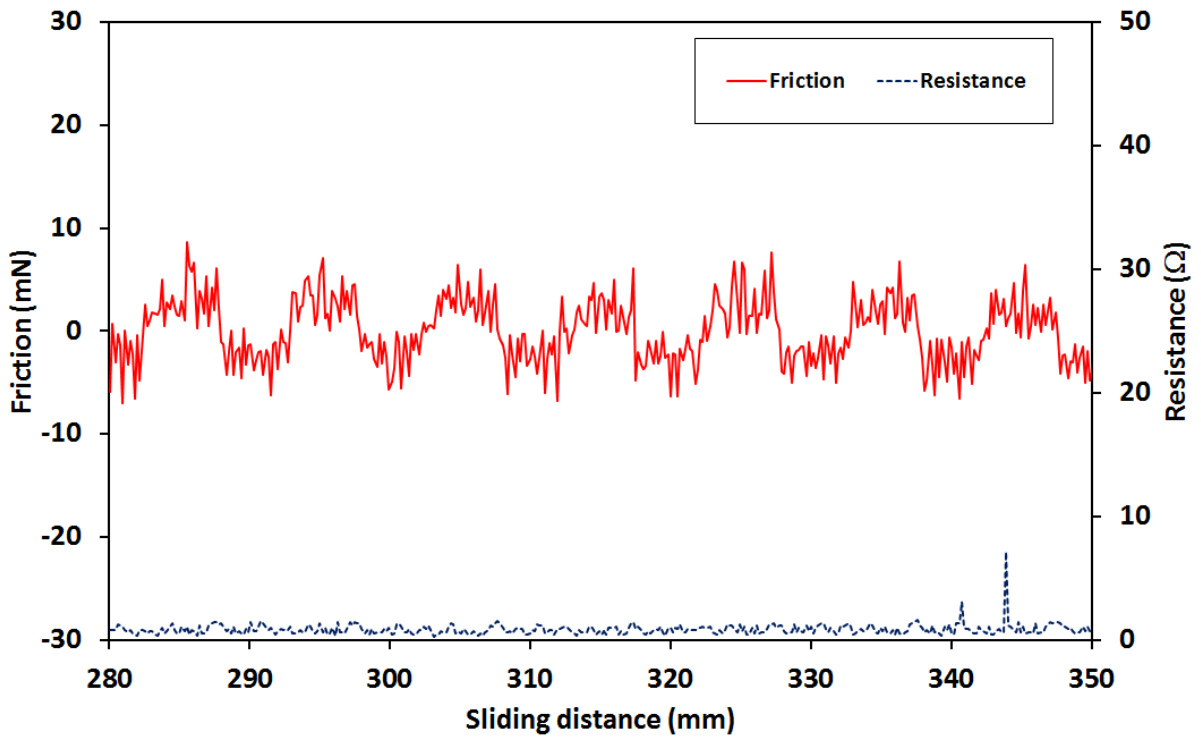
4(f)



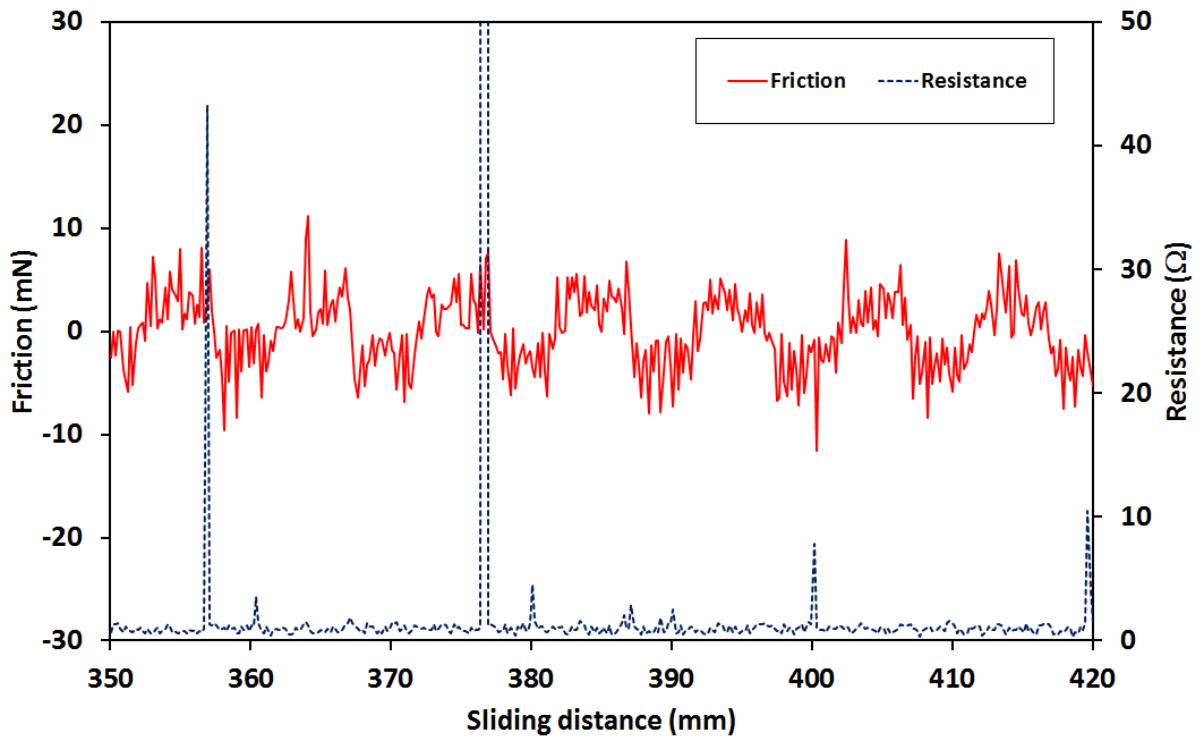
5(a)



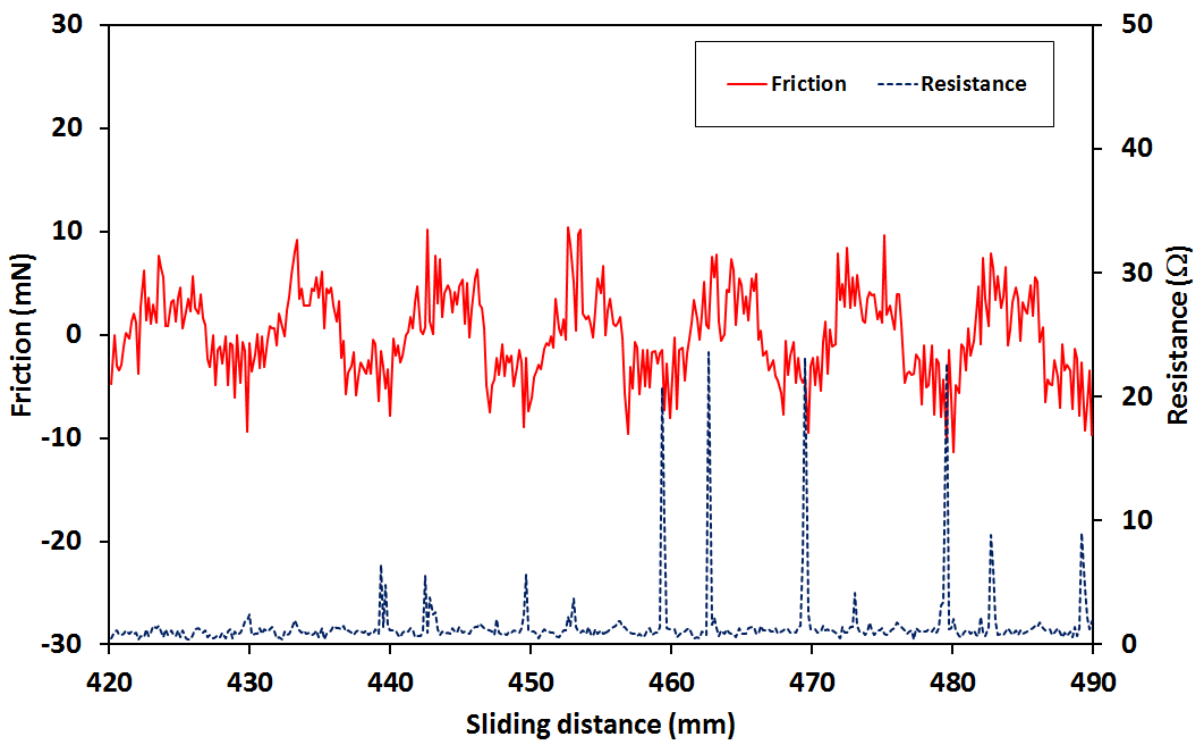
5(b)



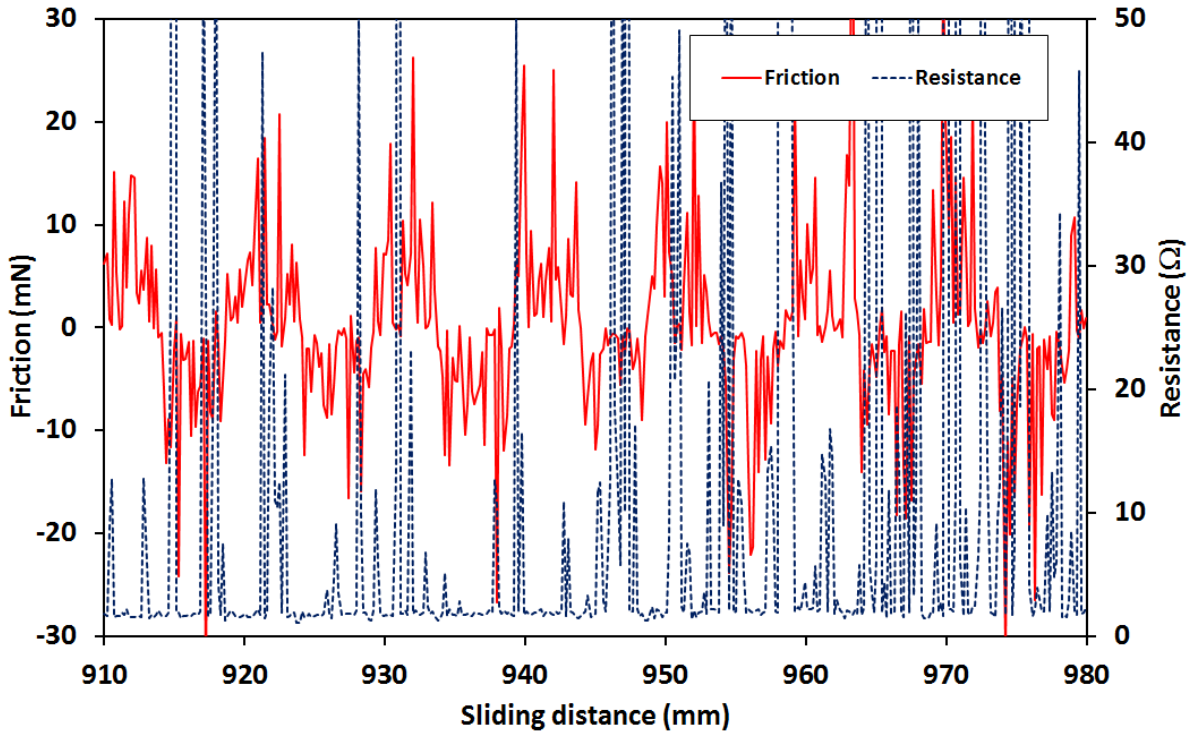
6(a)



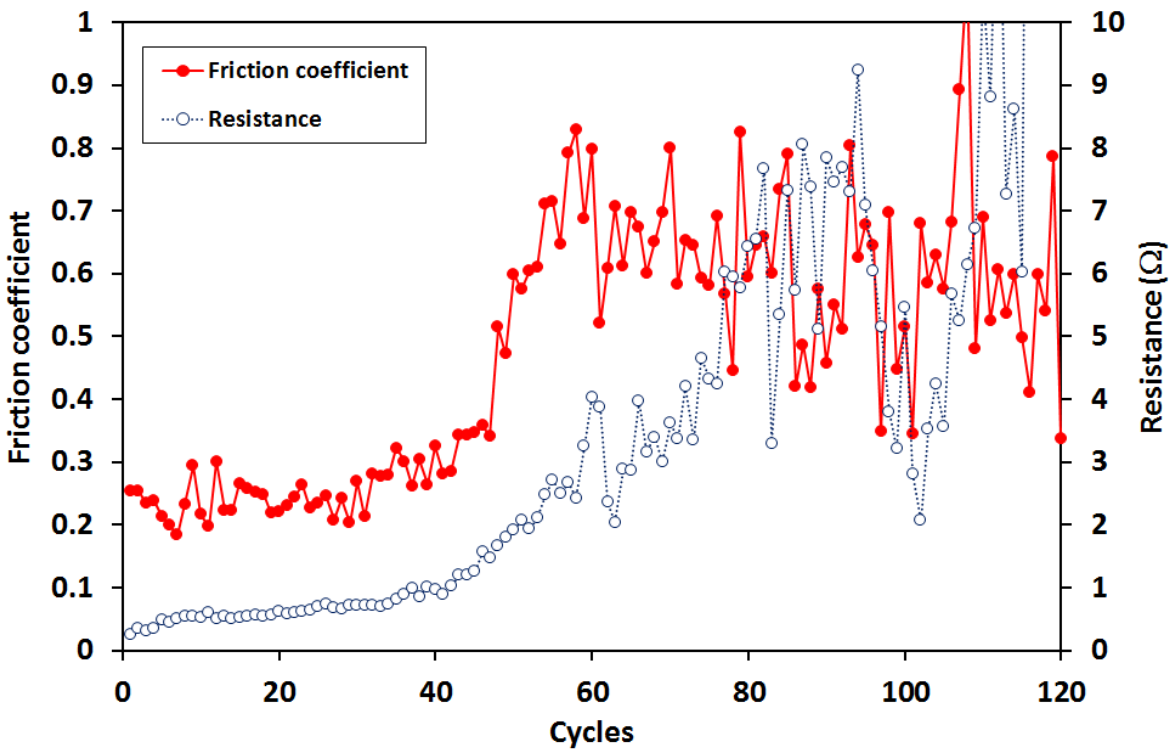
6(b)



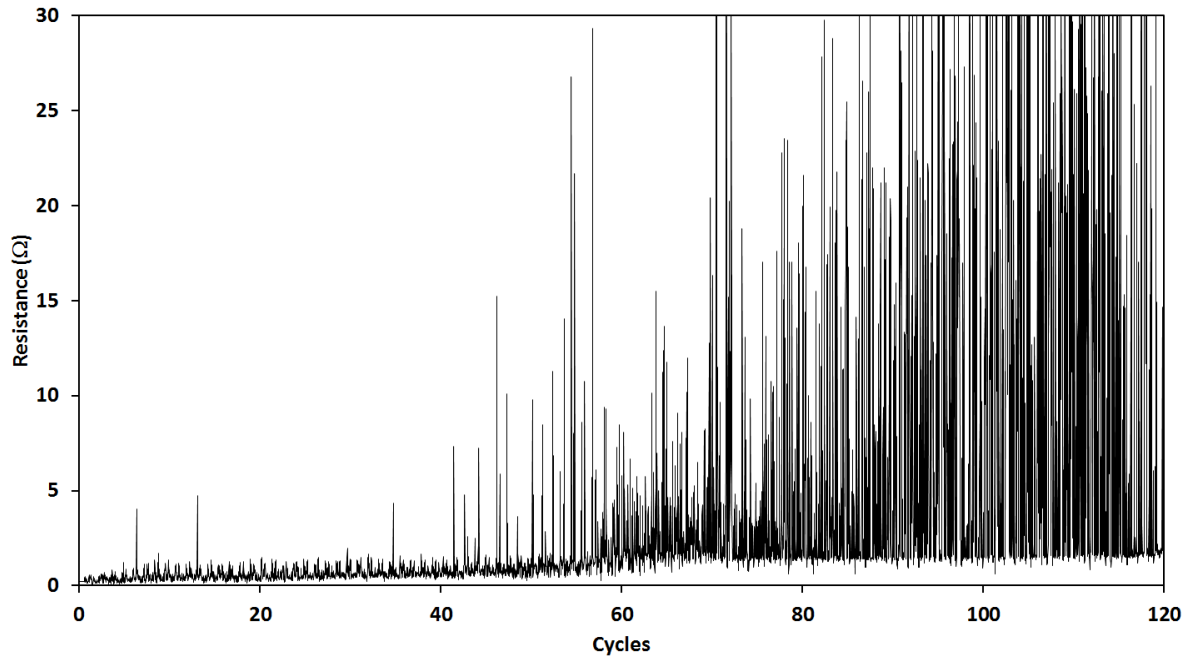
6 (c)



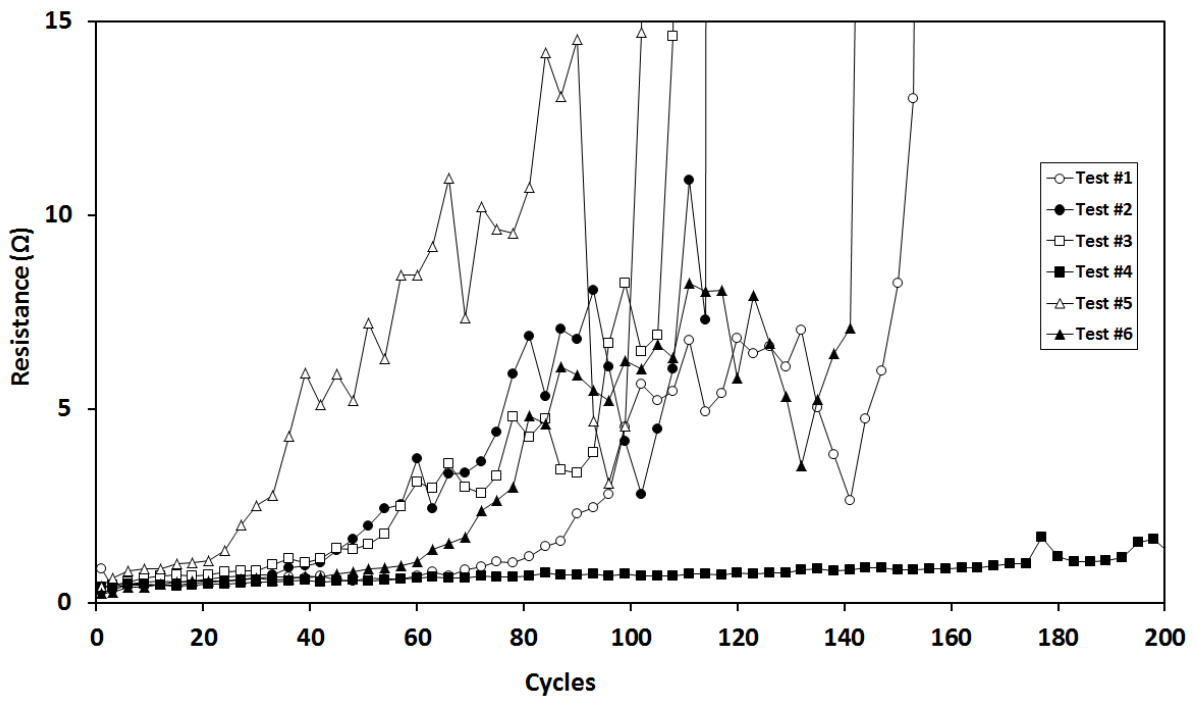
6 (d)



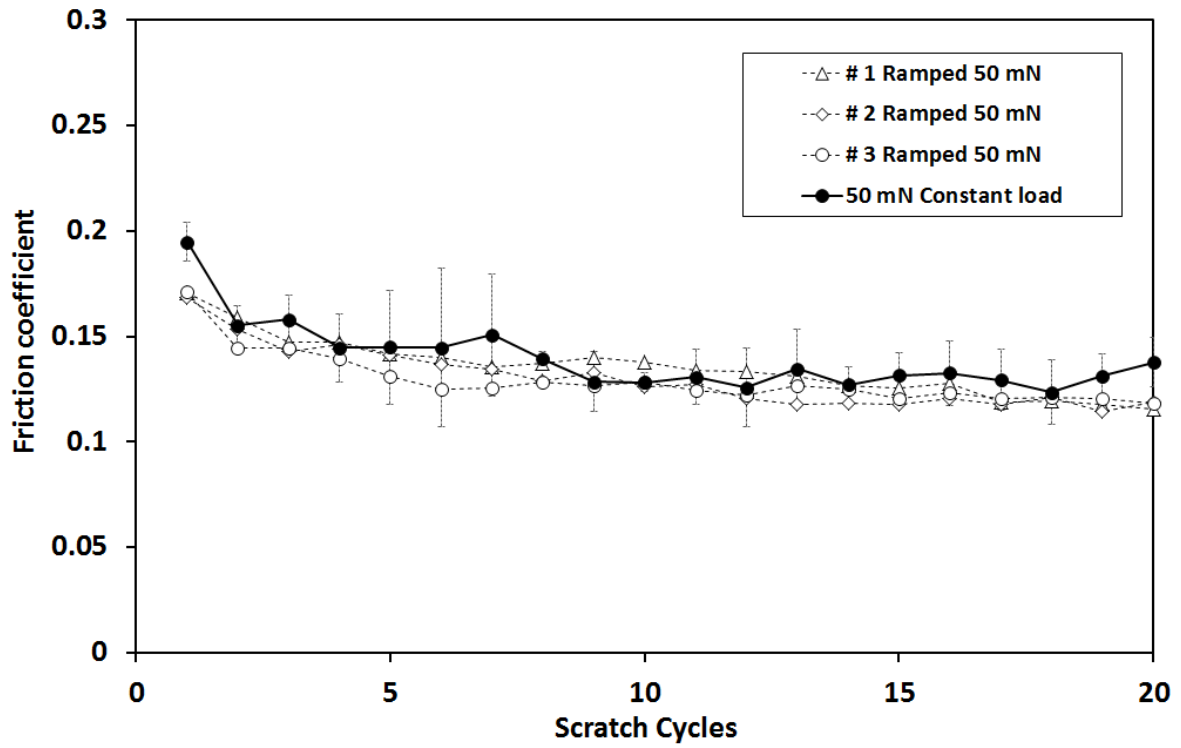
6 (e)



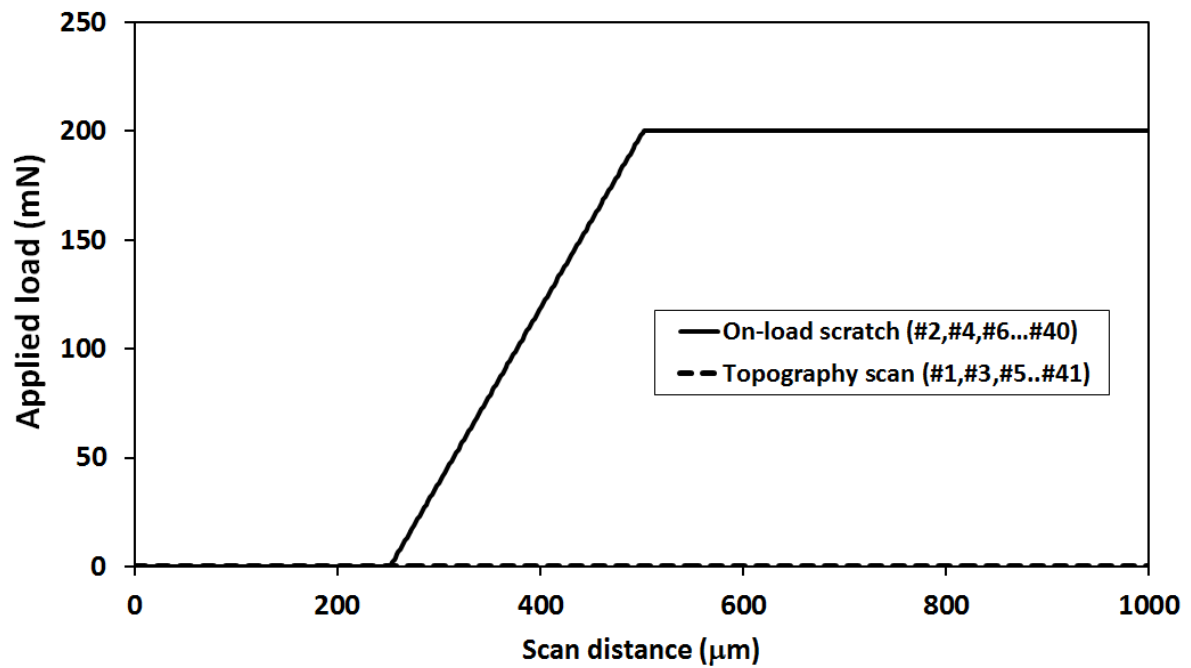
6 (f)



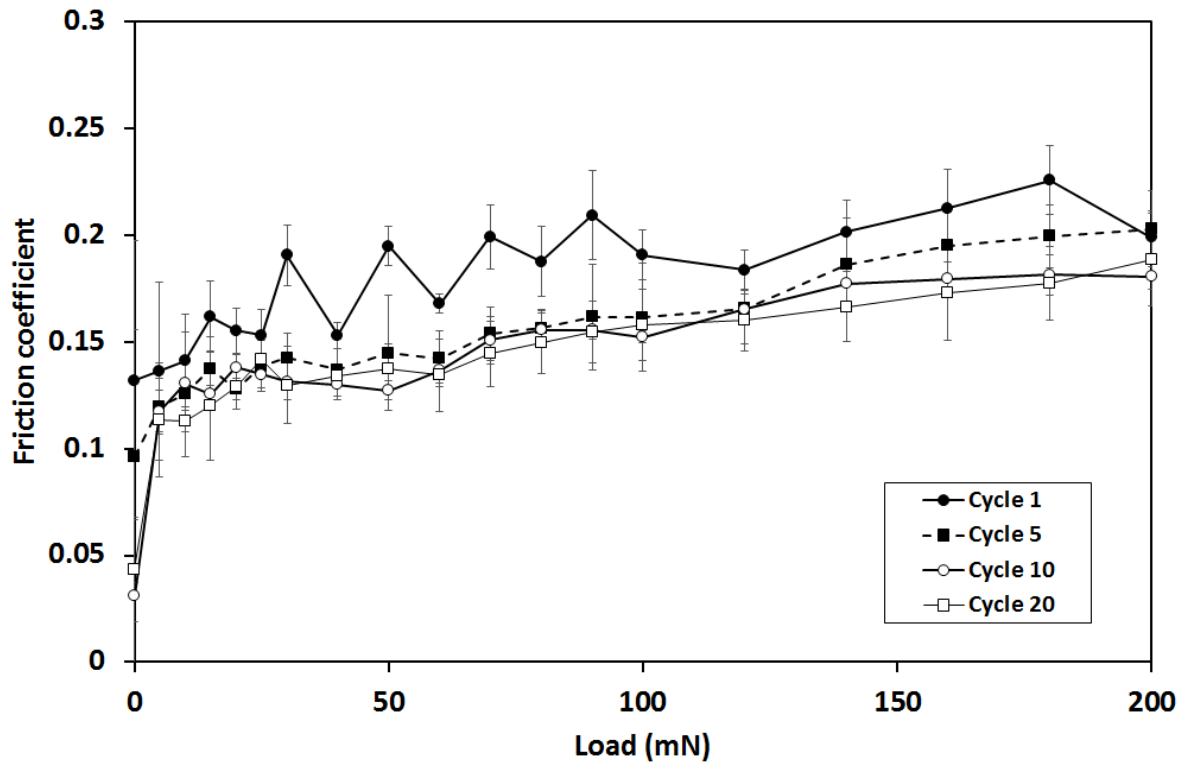
6 (g)



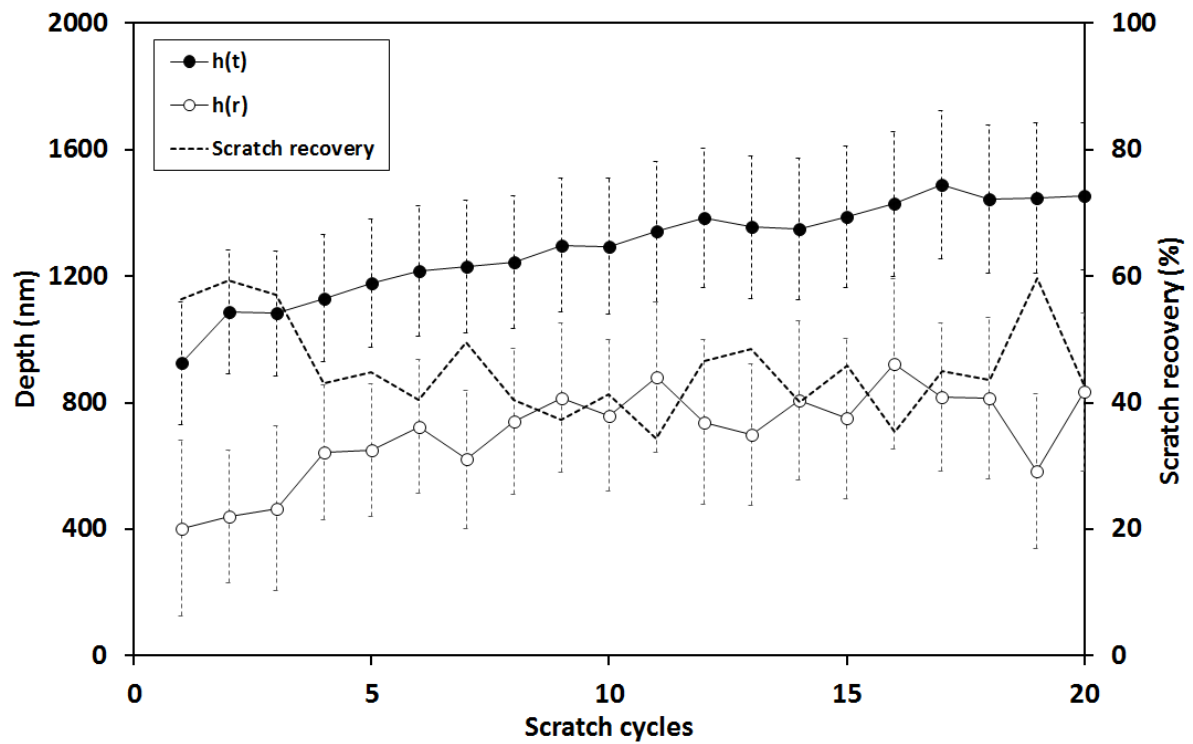
7 (a)



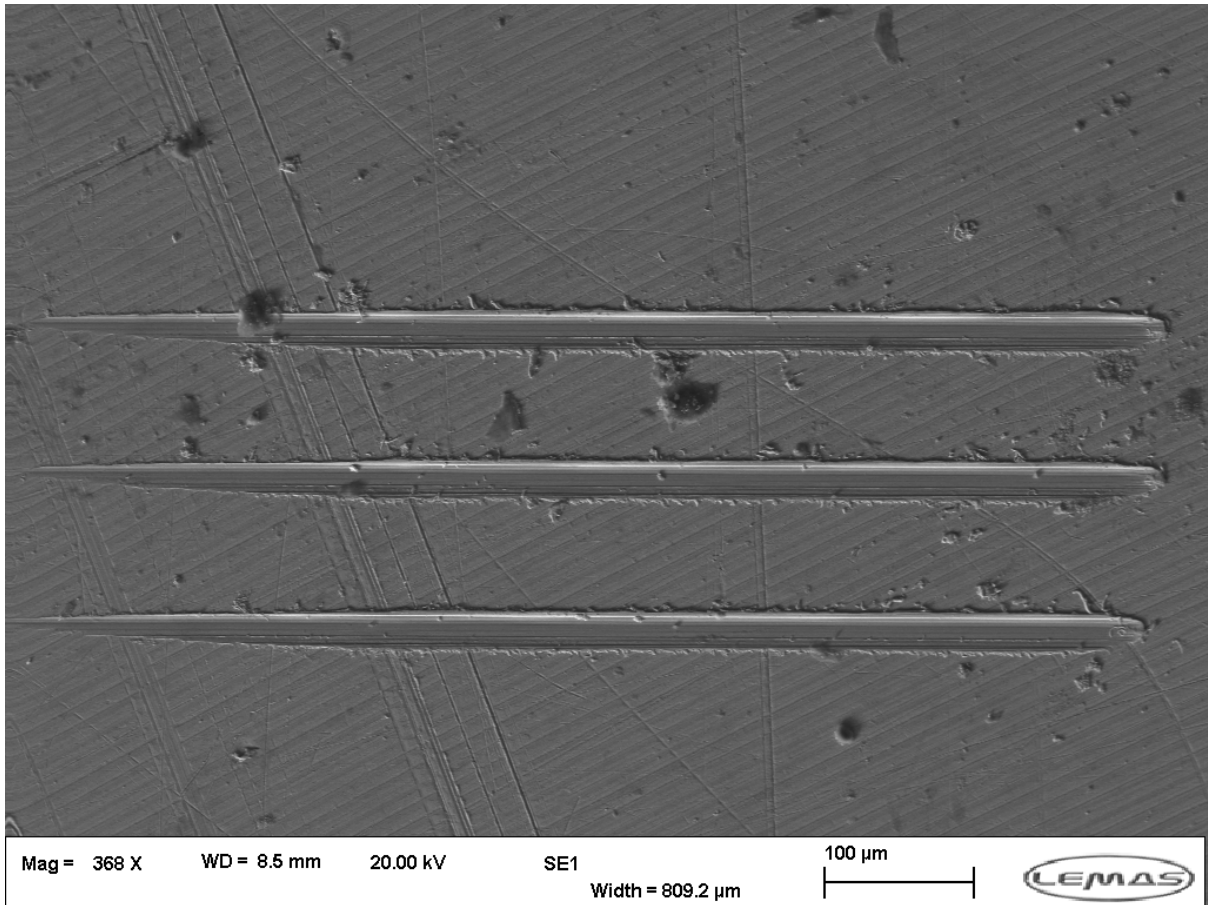
7 (b)



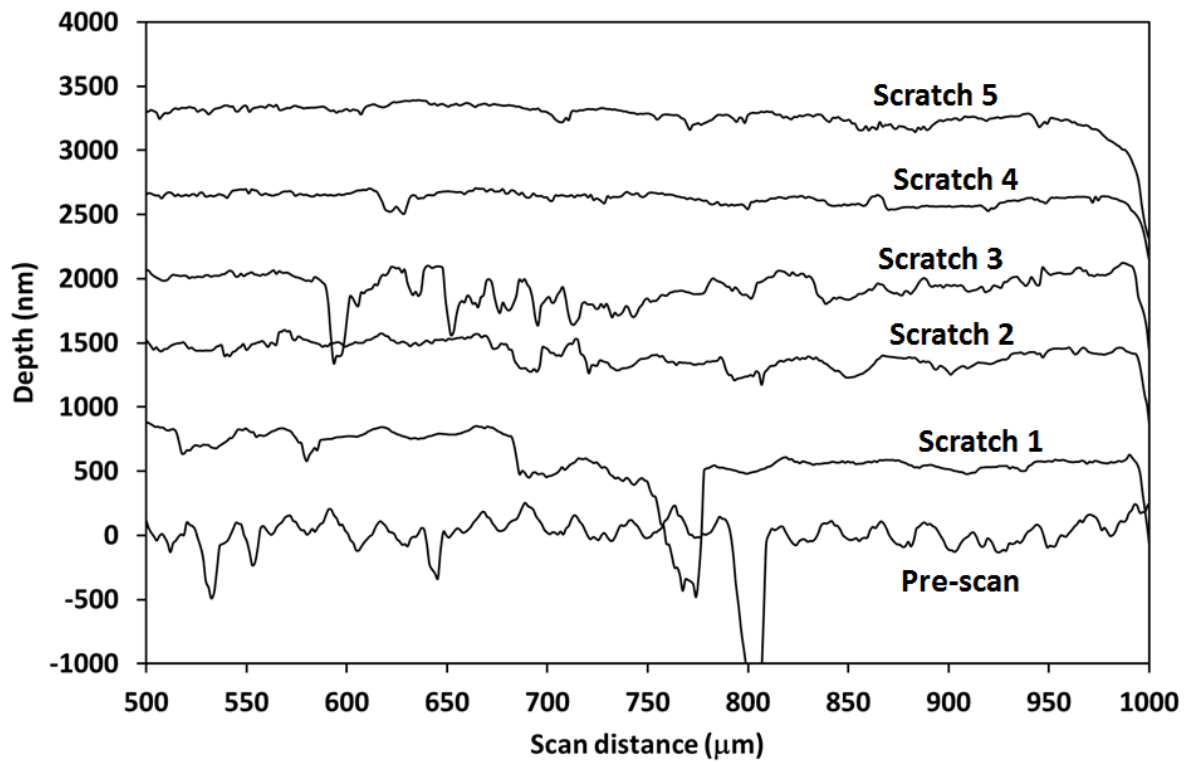
7 (c)



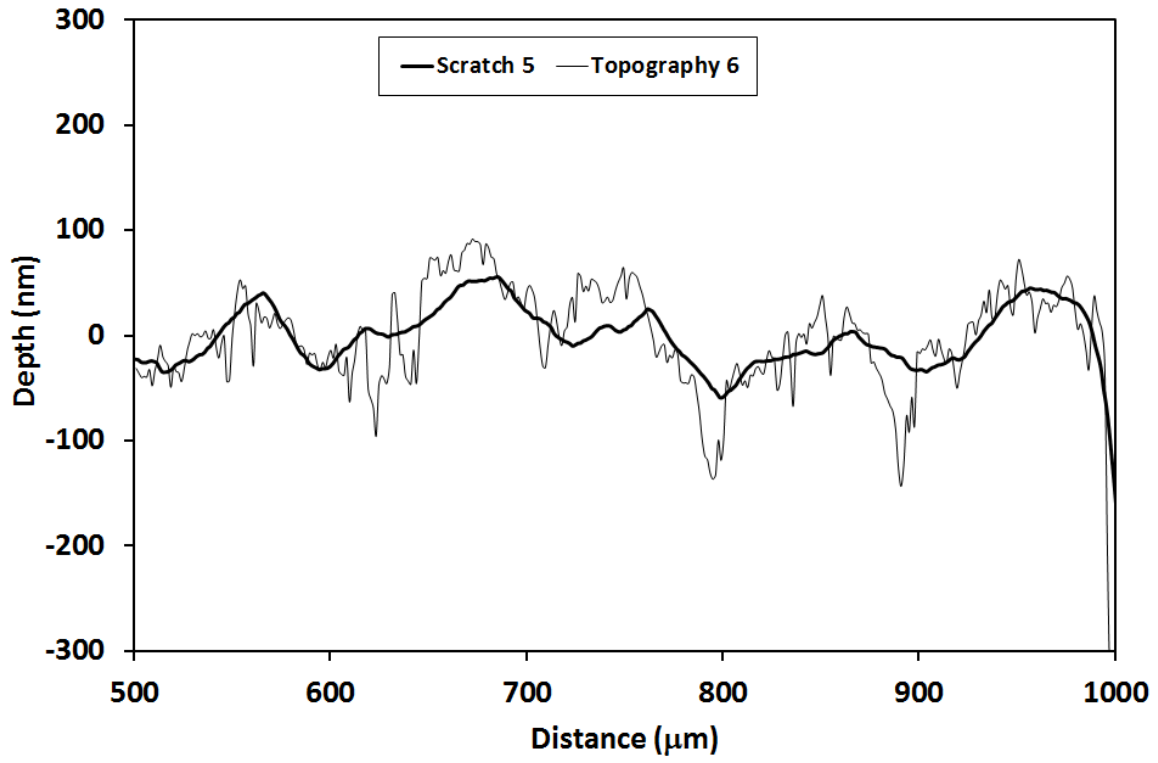
7 (d)



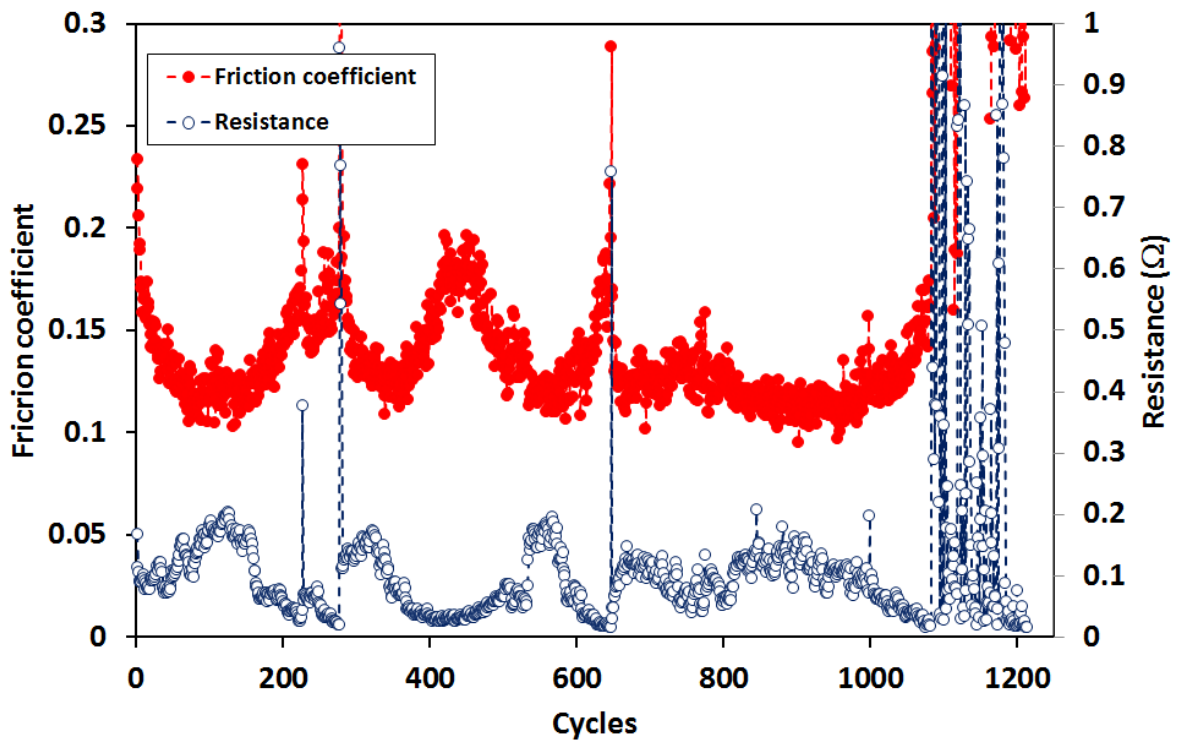
7 (e)



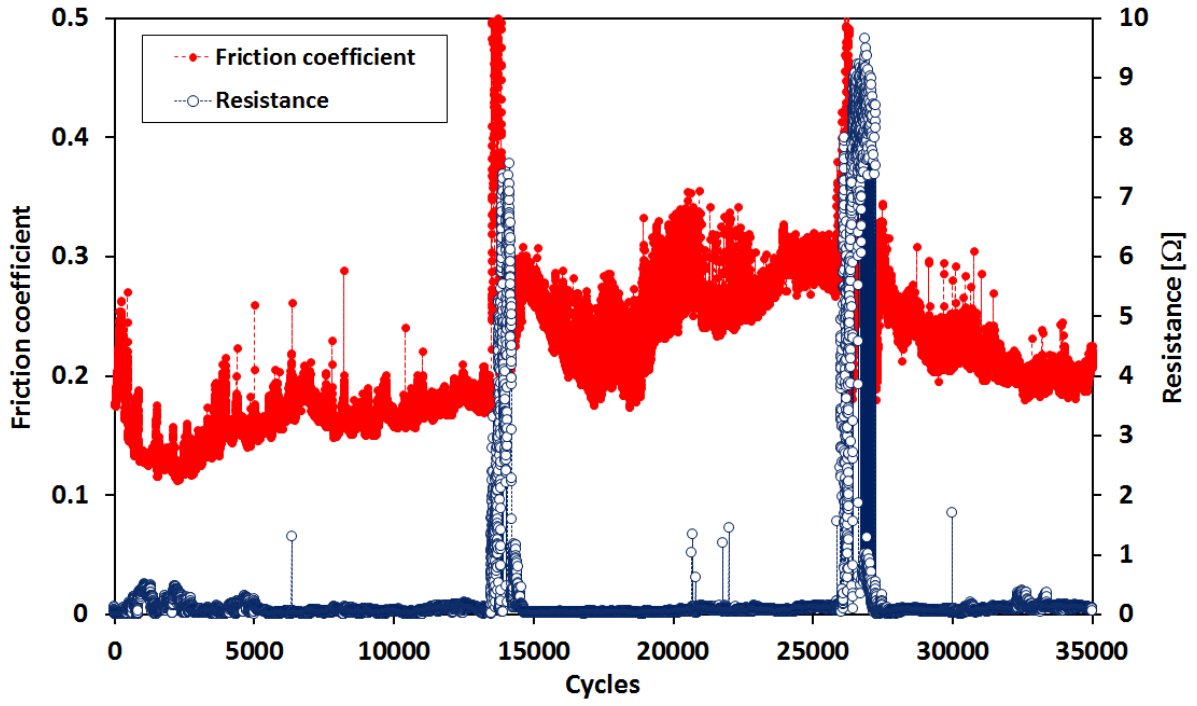
7 (f)



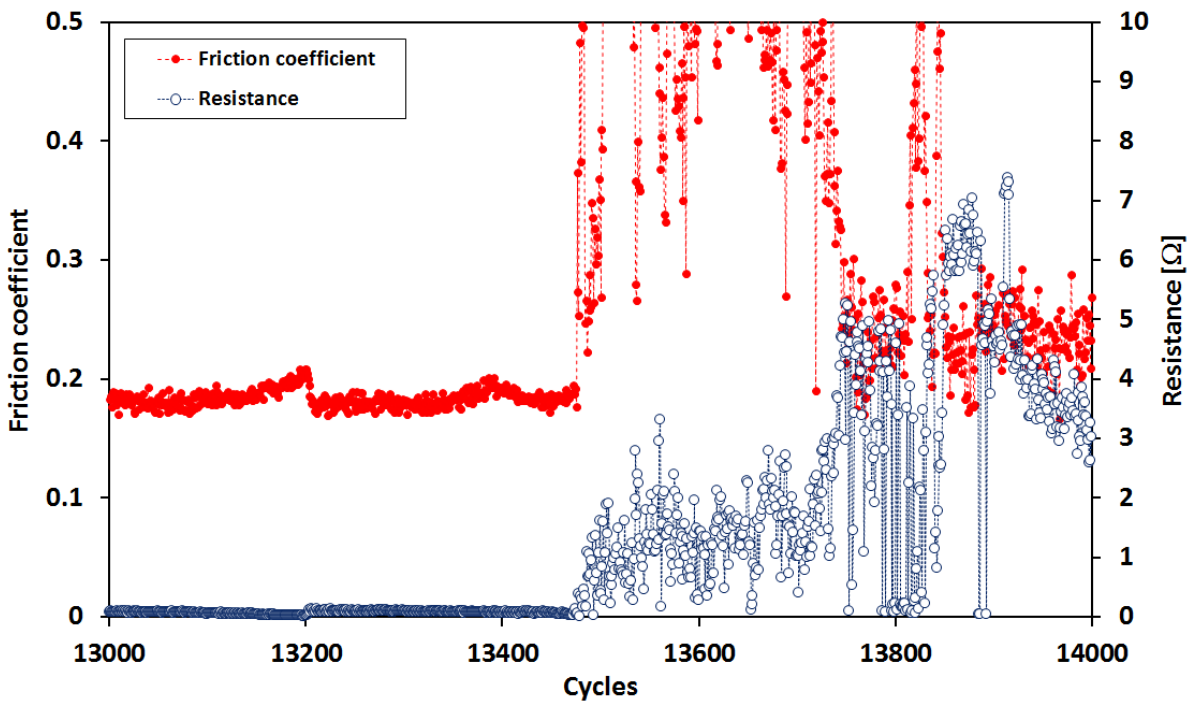
7 (g)



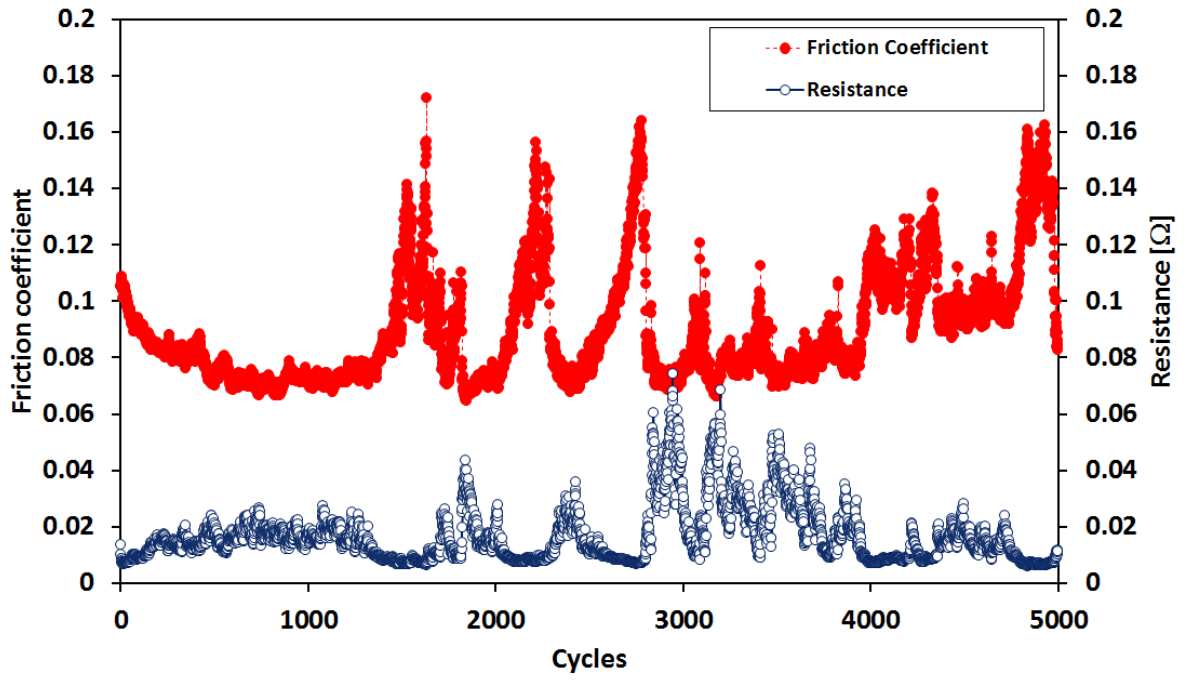
8 (a)



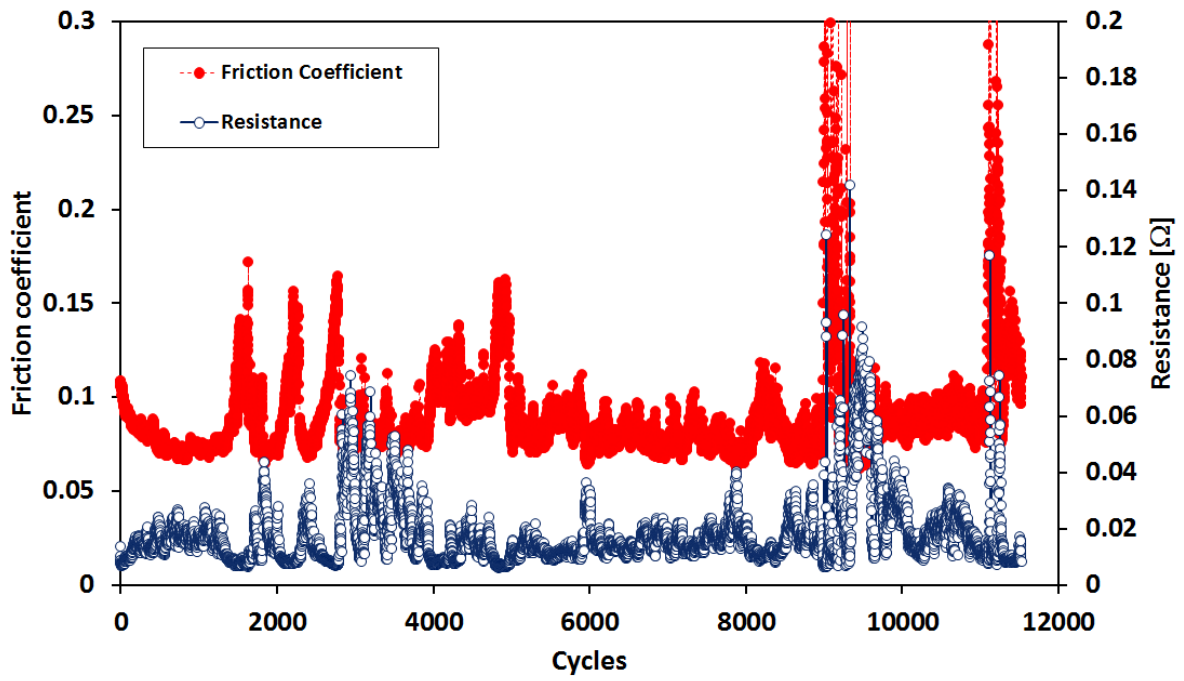
8 (b)



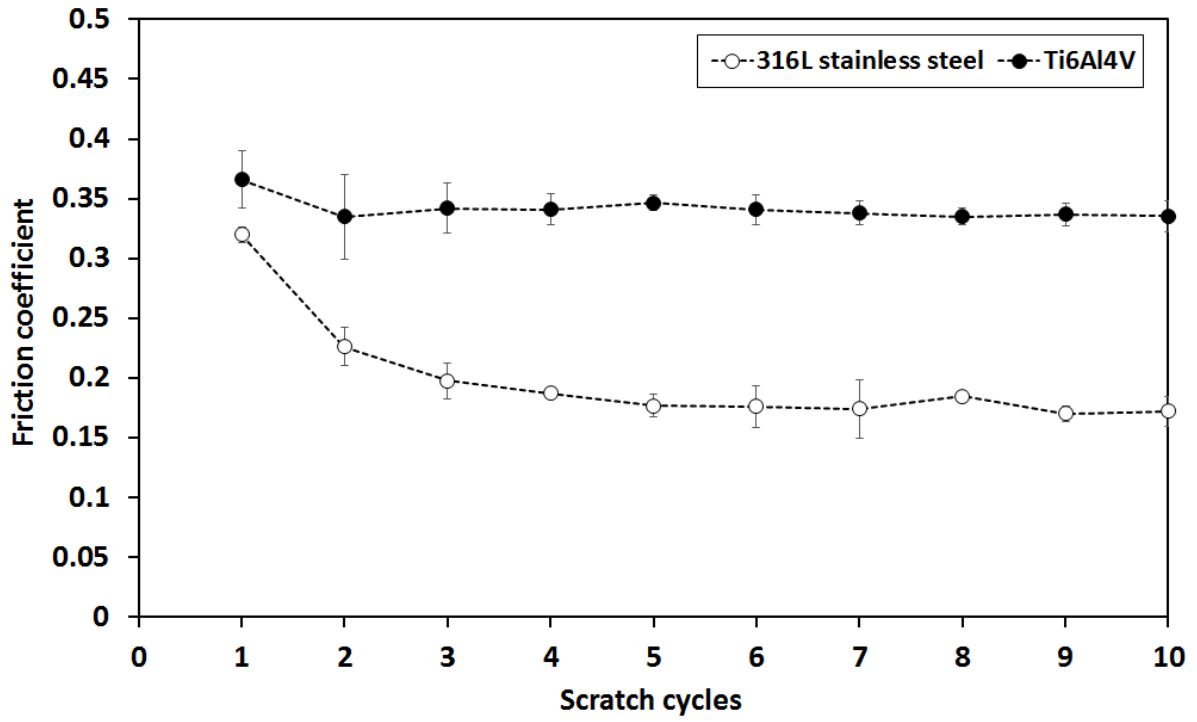
8 (c)



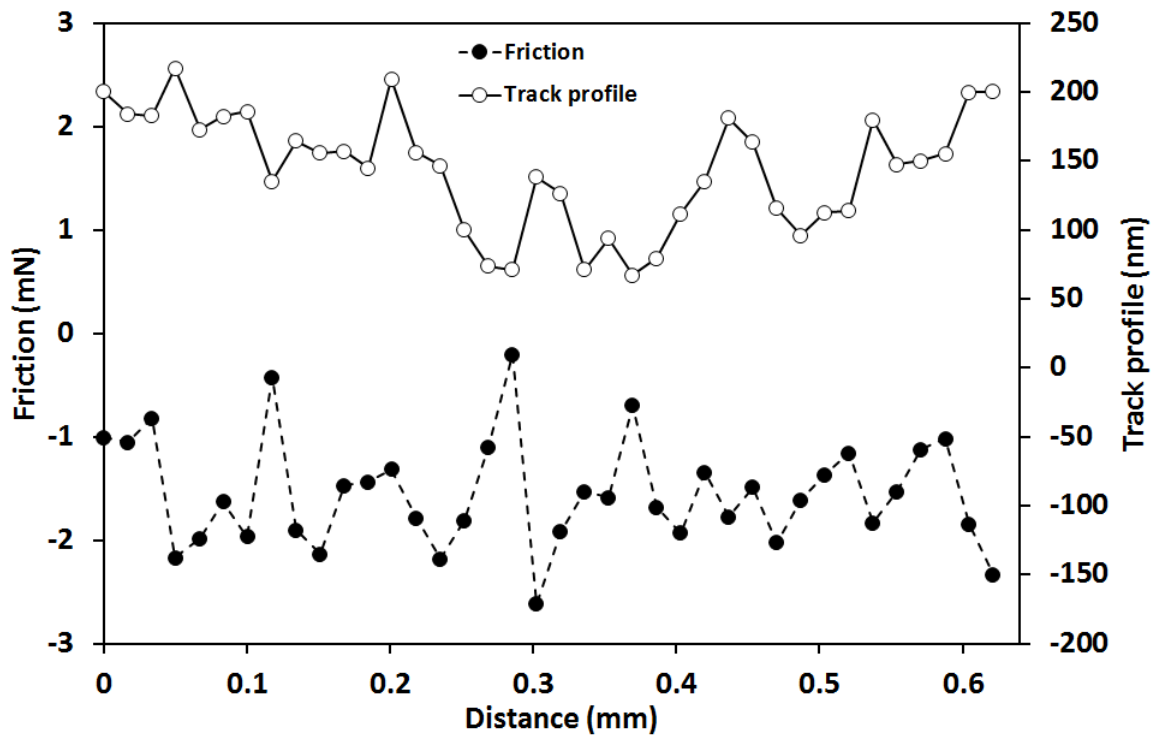
8 (d)



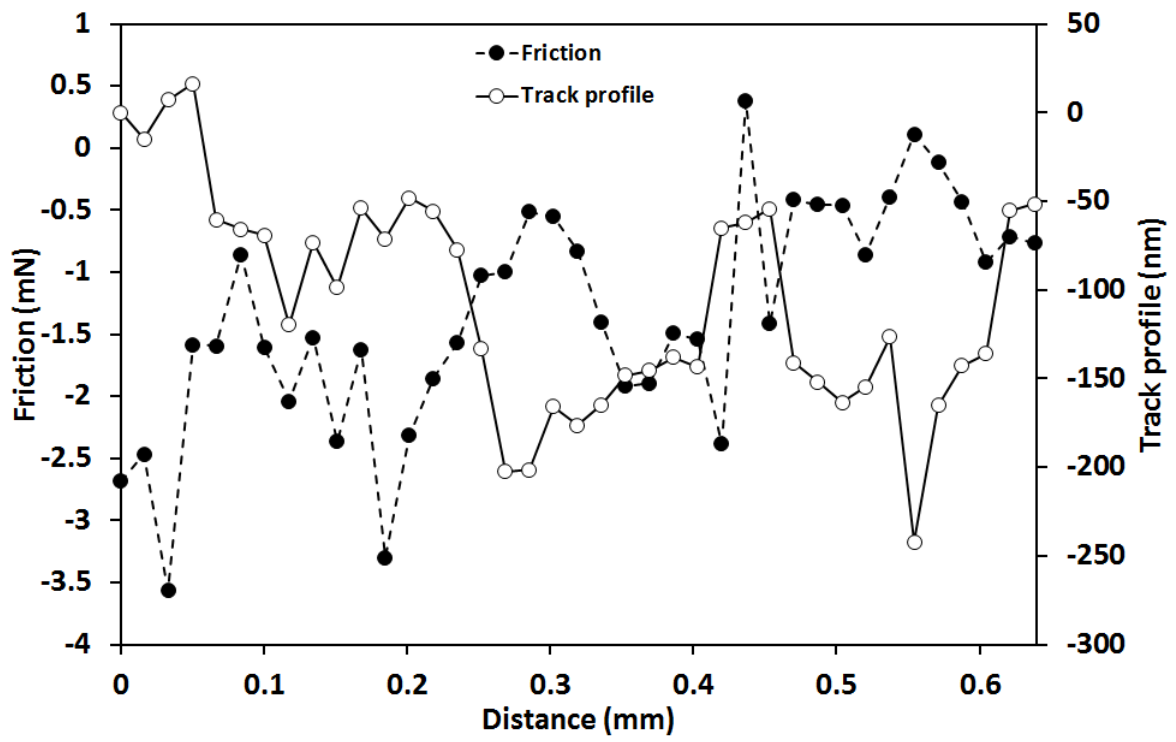
8 (e)



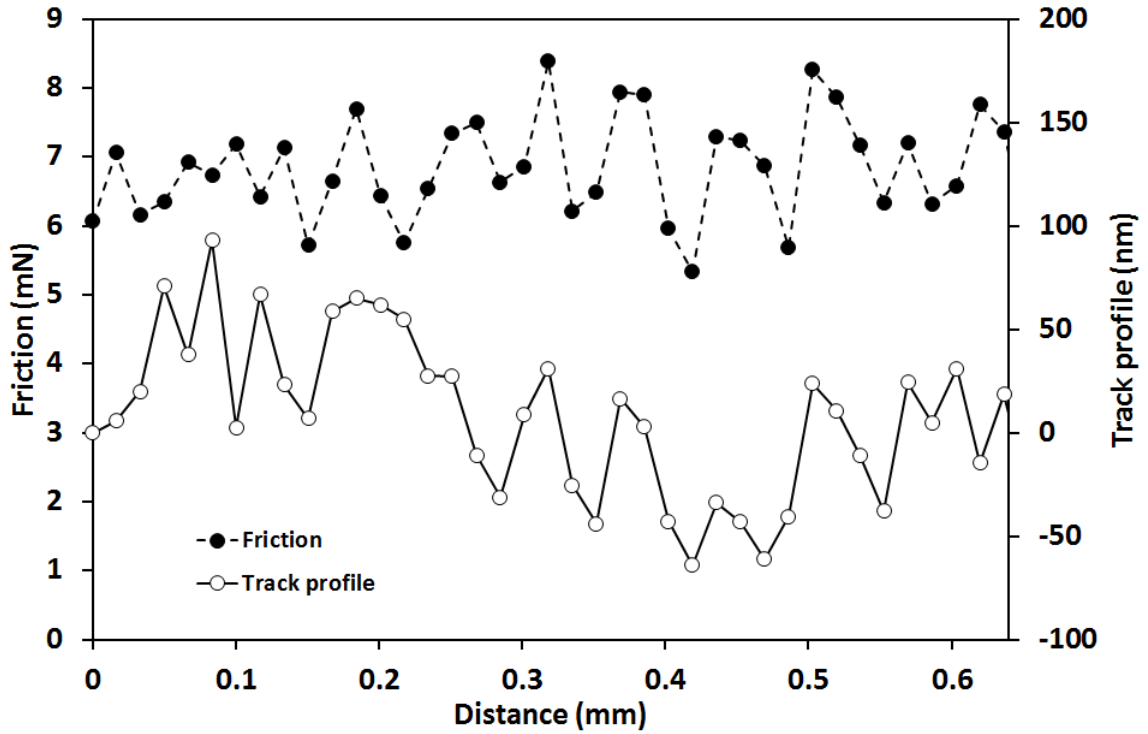
9.



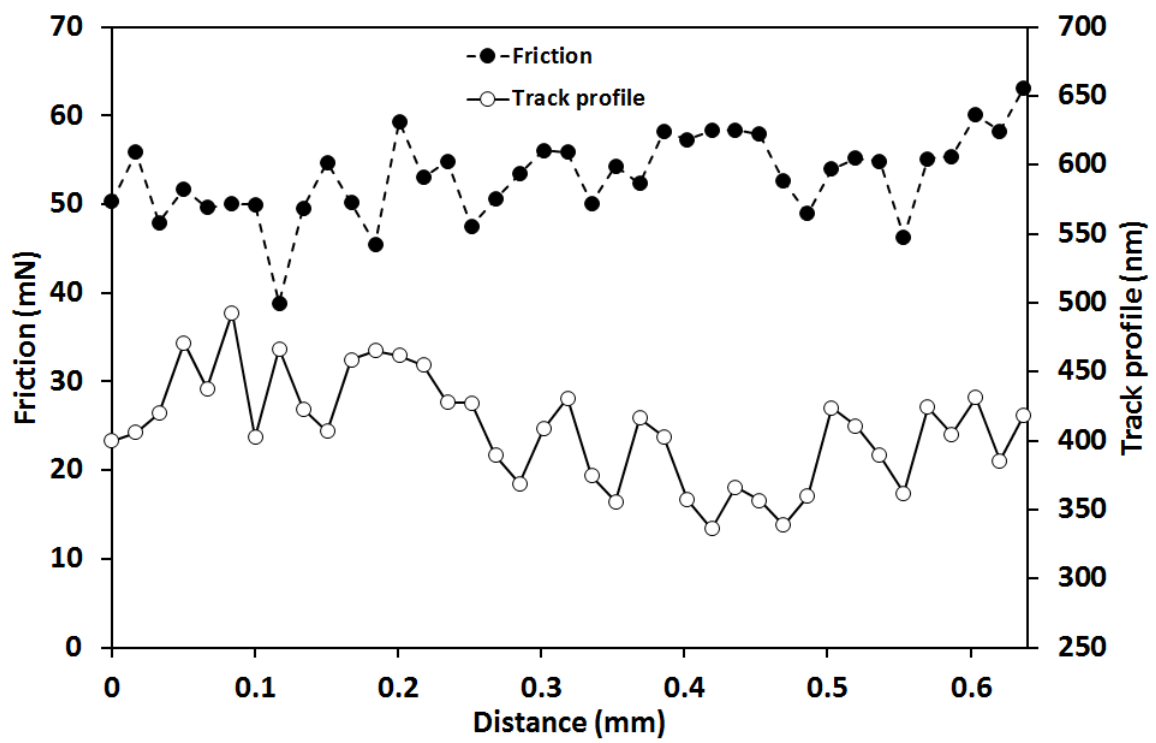
10 (a)



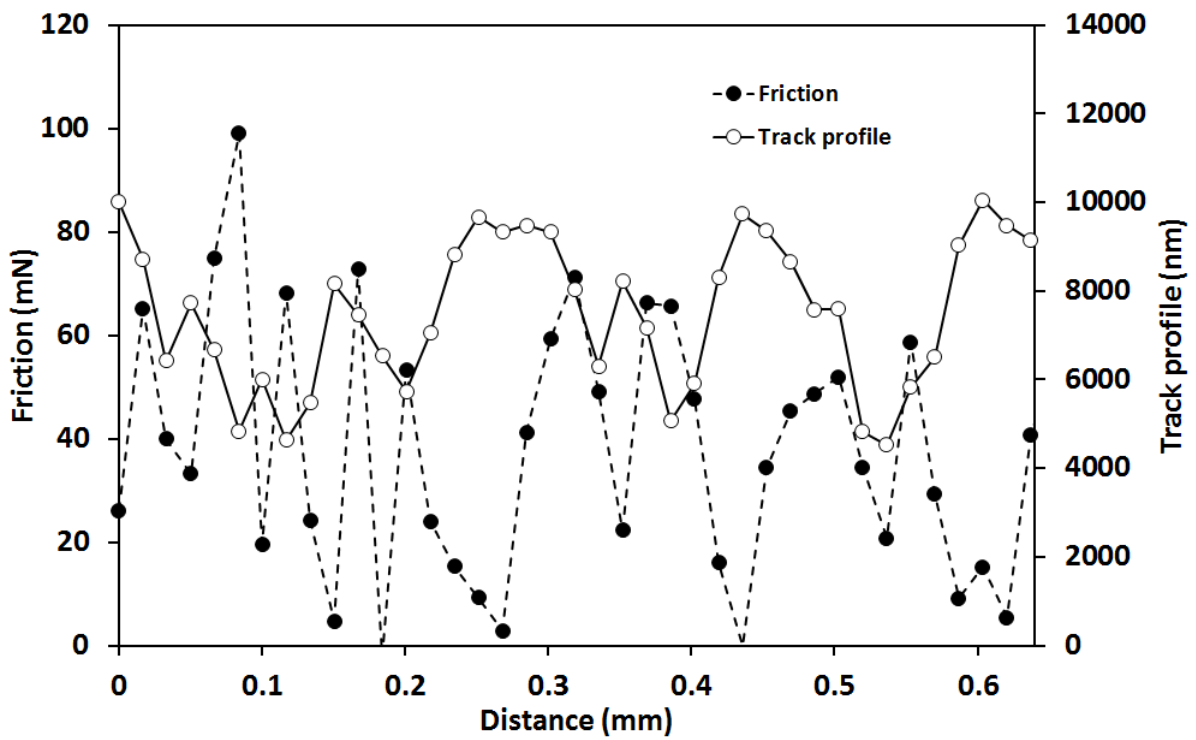
10 (b)



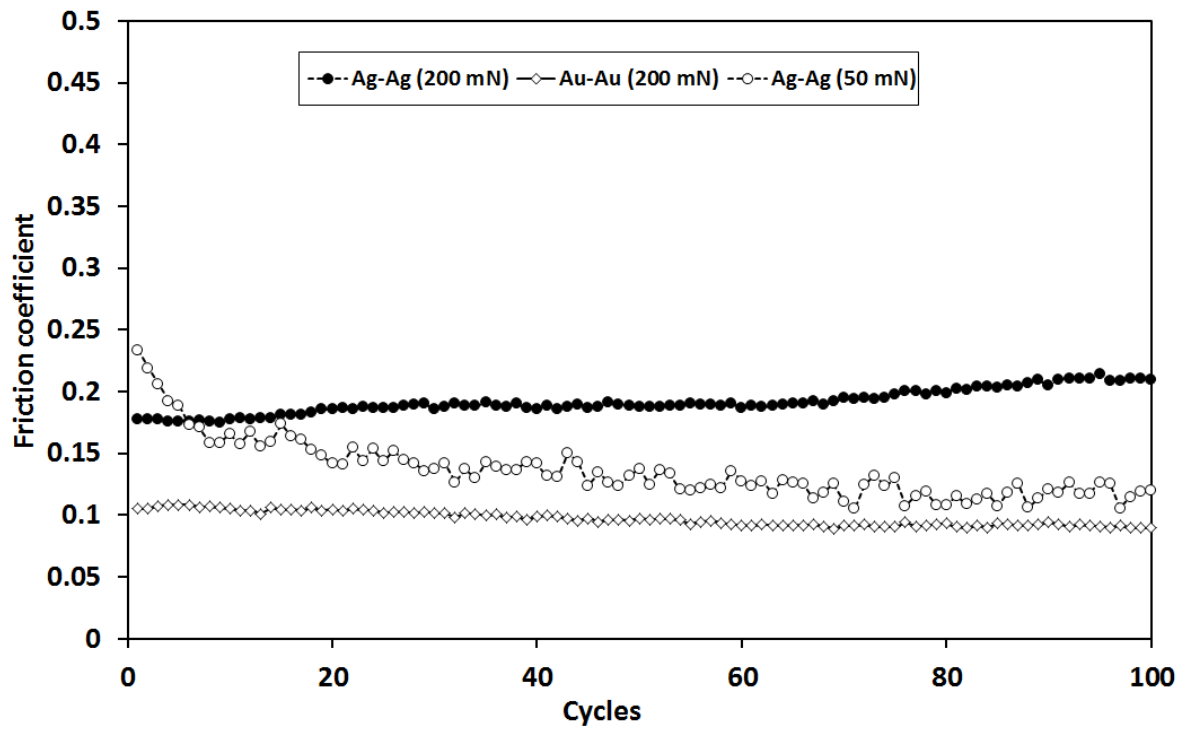
10 (c)



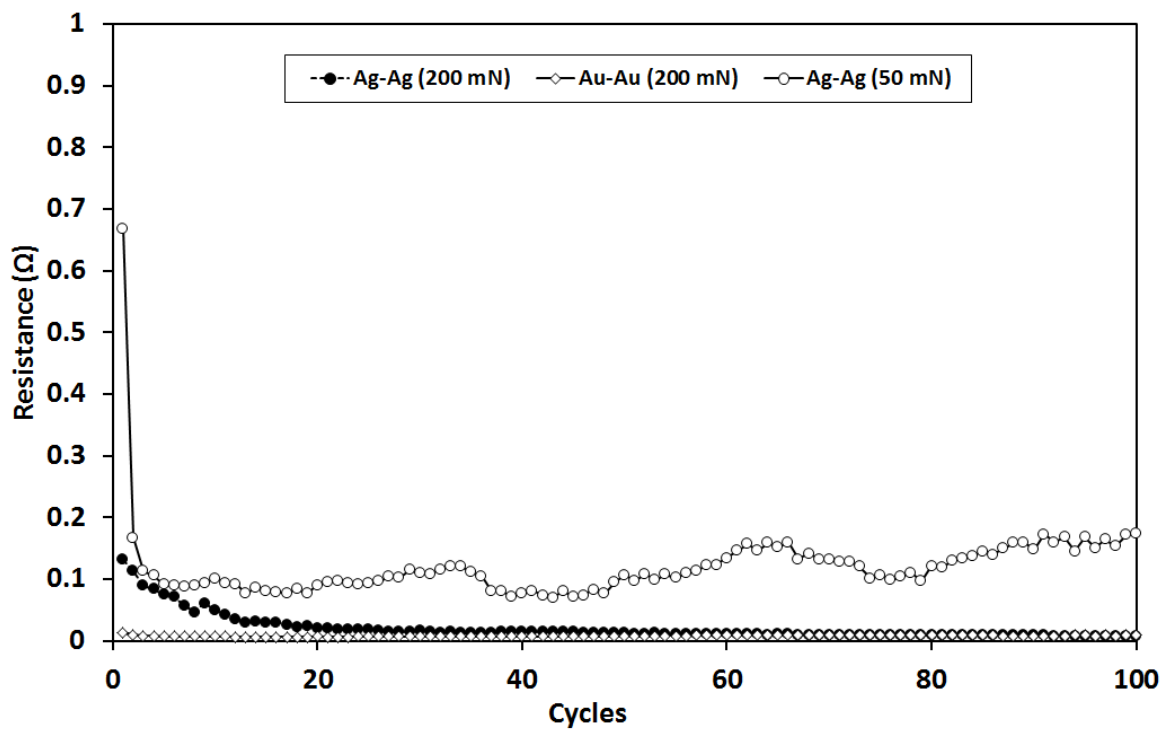
10 (d)



10 (e)



11 (a)



11 (b)